Bull Volcanol (2011) 73:1427–1454
DOI 10.1007/s00445-011-0459-y

RESEARCH ARTICLE

A re-appraisal of the stratigraphy and volcanology of the Cerro Galán volcanic system, NW Argentina

Chris B. Folkes · Heather M. Wright · Raymond A. F. Cas · Shanaka L. de Silva · Chiara Lesti · Jose G. Viramonte

Received: 15 February 2009 / Accepted: 31 January 2011 / Published online: 6 May 2011

Abstract From detailed fieldwork and biotite $^{40}Ar/^{39}Ar$ dating correlated with paleomagnetic analyses of lithic clasts, we present a revision of the stratigraphy, areal extent and volume estimates of ignimbrites in the Cerro Galán volcanic complex. We find evidence for nine distinct outflow ignimbrites, including two newly identified ignimbrites in the Toconquis Group (the Pitas and Vega Ignimbrites). Toconquis Group Ignimbrites (~5.60–4.51 Ma biotite ages) have been discovered to the southwest and north of the caldera, increasing their spatial extents from previous estimates. Previously thought to be contemporaneous, we distinguish the Real Grande Ignimbrite (4.68±0.07 Ma biotite age) from the Cueva Negra Ignimbrite (3.77± 0.08 Ma biotite age). The form and collapse processes of the Cerro Galán caldera are also reassessed. Based on re-interpretation of the margins of the caldera, we find evidence for a fault-bounded trapdoor collapse hinged along a regional N-S fault on the eastern side of the caldera and accommodated on a N-S fault on the western caldera margin. The collapsed area defines a roughly isosceles trapezoid shape elongated E-W and with maximum dimensions 27×16 km. The Cerro Galán Ignimbrite (CGI; 2.08±0.02 Ma sanidine age) outflow sheet extends to 40 km in all directions from the inferred structural margins, with a maximum runout distance of ~80 km to the north of the caldera. New deposit volume estimates confirm an increase in eruptive volume through time, wherein the Toconquis Group Ignimbrites increase in volume from the ~10 km^3 Lower Merihuaca Ignimbrite to a maximum of ~390 km^3 (Dense Rock Equivalent; DRE) with the Real Grande Ignimbrite. The climactic CGI has a revised volume of ~630 km^3 (DRE), approximately two thirds of the commonly quoted value.

Keywords Cerro Galán · $^{40}Ar/^{39}Ar$ · Ignimbrite volumes · Caldera collapse · Trapdoor

Editorial responsibility: K. Cashman

This paper constitutes part of a special issue:

Cas RAF, Cashman K (eds) The Cerro Galan Ignimbrite and Caldera: characteristics and origins of a very large volume ignimbrite and its magma system.

Electronic supplementary material The online version of this article (doi:10.1007/s00445-011-0459-y) contains supplementary material, which is available to authorized users.

C. B. Folkes (✉) · H. M. Wright · R. A. F. Cas
School of Geosciences, Monash University,
Building 28,
Victoria 3800, Australia
e-mail: chris.folkes@monash.edu

H. M. Wright
US Geological Survey MS 910,
Menlo Park, CA 94025, USA

S. L. de Silva
Department of Geosciences, Oregon State University,
Corvallis, OR 97331, USA

C. Lesti
Universitá Roma Tre,
Largo S. Leonardo Murialdo,
1-00146 Roma, Italy

J. G. Viramonte
Univesidad Nacional de Salta,
Instituto GEONORTE and CONICET,
Av. Bolivia 5150,
Salta 4400, Argentina

Introduction

The Cerro Galán caldera, located in northwestern Argentina in the Central Volcanic Zone (CVZ) of the Andean

continental margin volcanic arc of South America, is often cited as the product of one of the largest caldera-forming 'super-eruptions' on Earth (e.g., Mason et al. 2004). No super-eruptions have been witnessed in human history and little is known about their frequency, eruption mechanisms or the emplacement processes of erupted material. Previous work has shown that at least one VEI 8 eruption occurred at Cerro Galán since 2.5 Ma (Francis et al. 1983). In addition, a sequence of large volume pyroclastic eruptions preceded this cataclysmic eruption (Sparks et al. 1985). Therefore, the time transgressive sequence of pyroclastic deposits from Cerro Galán provides information about the long term evolution of large-volume magma chambers.

The CVZ has been the site of numerous large-volume silicic ignimbrite eruptions since ~10 Ma (Guest 1969; Sparks et al. 1985; Gardeweg and Ramirez 1987; Ort 1993; Coira et al. 1996; Kay et al. 1999; Soler et al. 2007). The highest concentration of these large-volume ignimbrites in the CVZ is in the Altiplano-Puna Volcanic Complex (APVC; Fig. 1), covering ~70,000 km^2 and comprising >10,000 km^3 of crystal-rich dacitic ignimbrites emplaced during late Miocene to Pleistocene time (de Silva and Francis 1989; de Silva 1989a, b; Lindsay et al. 2001). In the APVC, magma supply rates are high, and large chamber volumes are inferred to have developed over hundreds of thousands of years (de Silva and Gosnold 2007).

The Cerro Galán volcanic system, which lies ~200 km south of the APVC (Altiplano-Puna Volcanic Complex; Fig. 1), is a classic example of a long-lived silicic magmatic system (e.g., Mason et al. 2004). The cataclysmic supervolcanic eruption of the ~2.1 Ma Cerro Galán Ignimbrite (CGI) has previously been proposed to have been of the same order of magnitude as the eruption that produced the Fish Canyon Tuff (e.g., Sparks et al. 1985), currently thought to have been the largest explosive eruption on Earth (Mason et al. 2004). Furthermore, the total volume of pre-2.1 Ma pyroclastic eruption was thought to total half of the CGI volume (Sparks et al. 1985). No modern, systematic and detailed investigation into the stratigraphic and age relationships or eruption mechanisms of the eruption sequence has, however, been completed despite significantly better access since the first seminal work on the system by Francis, Sparks and co-workers in the late 1970's and early 1980's. We have revisited this classic system to further investigate the eruption mechanisms and emplacement of large volume ignimbrites and the development of long-lived, large volume silicic systems. In this paper we focus on the stratigraphy of the ignimbrite succession associated with the Cerro Galán volcanic system. Using new field mapping and stratigraphic evidence, coupled with $^{40}Ar/^{39}Ar$ age determinations and paleomagnetic evidence,

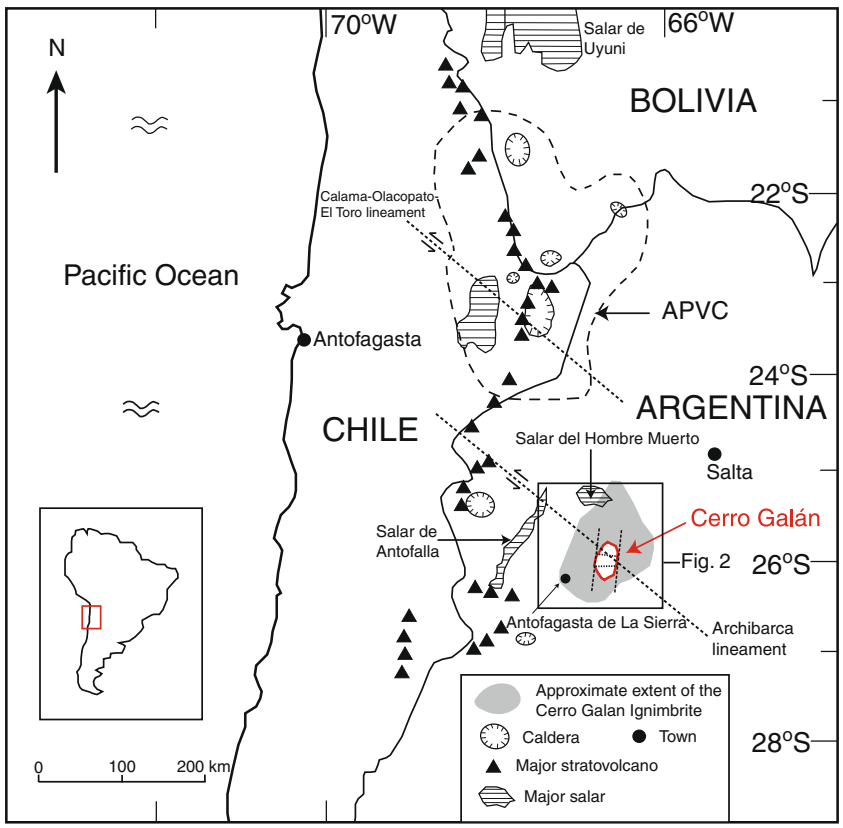

Fig. 1 Regional setting of the Cerro Galán caldera and its associated ignimbrites. The Altiplano-Puna Volcanic Complex (APVC), regional strike-slip lineaments and the location of Fig. 2 are also shown

we present an updated stratigraphy, a more complete set of ignimbrite distribution maps and more-accurate estimations of distributions and volumes for each ignimbrite. Using new $^{40}Ar/^{39}Ar$ age determinations, we have identified new ignimbrites (the Pitas and Vega Ignimbrites) and separated others that were previously thought to have erupted concurrently (e.g., the Real Grande and Cueva Negra Ignimbrites). A reinterpretation of the caldera collapse and structure is presented, and we quantify and improve the assumptions that are involved in calculating realistic volume estimates for the original erupted ignimbrites. In aggregate, these data elucidate the temporal evolution of the Cerro Galán magmatic system, allowing it to be put in context with other large silicic magmatic systems.

Cerro Galán Caldera—previous work

The Cerro Galán caldera was first identified in the late 1970's using satellite images from the Central Andes (Friedman and Heiken 1977; Francis and Baker 1978). The caldera (25°55′S 66°52′W) is located in the Puna region of the southern CVZ of the South American Andes (Fig. 1), approximately 200 km south of the southern margin of the Altiplano-Puna Volcanic complex (APVC). The caldera complex is situated at the SE end of the Archibarca Lineament—a NW-SE striking regional strike-slip fault that is part of a sub-parallel fault series thought to have been formed via transtensional activity related to overthickening of the local lithosphere in this part of the Puna plateau (Viramonte et al. 1984; Salfity 1985; Viramonte and Petrinovic 1990; Riller et al. 2001). The margins of the caldera are bounded by two regional N-S oriented faults, ~20 km apart, which are thought to have controlled the location of caldera-bounding faults, and through which extrusion of magma was facilitated (Sparks et al. 1985; de Silva and Francis 1991). Coira et al. (1982) and Jordan et al. (1983) have shown the Cerro Galán region to be located at a transition between two segments of the Andean subduction zone; south of 28°S, the seismic zone is sub-horizontal, whereas north of 24°S, the seismic zone dips at 30°.

Francis and Baker (1978) were the first to identify Cerro Galán as a major resurgent caldera (estimated as a 35×20 km elliptical structure) surrounded by 2,000 km^2 of associated ignimbrite. These authors interpreted the central elevated structural dome within the caldera to have formed via post-caldera magmatic resurgence leading to up-doming of the caldera floor and the intracaldera ignimbrite fill. Various pre-caldera and post-caldera small-volume lava domes were also identified within the modern caldera. The most recent and extensive Cerro Galán Ignimbrite (CGI) was first examined by Francis et al. (1983), who characterized the ignimbrite as a crystal-rich but pumice and lithic-poor pyroclastic flow deposit comprising one massive flow unit, up to 120 m thick. A more detailed investigation of the Galán stratigraphy was performed by Sparks et al. (1985), who described an older sequence of ignimbrites. Rb-Sr age determinations on the CGI indicated an eruption age of 2.1 Ma (Table 1). Outflow deposits 20–300 m thick were estimated to reach up to 100 km from the caldera rim. Six ignimbrites were documented underlying the CGI, with a total thickness in excess of 250 m. Collectively, these pre-CGI ignimbrites were designated as the Toconquis Formation. They include the Blanco, Lower Merihuaca, Middle Merihuaca, Upper Merihuaca, Real Grande and Cueva Negra Ignimbrites, from oldest to youngest. The Toconquis Formation Ignimbrites were dated from ~6.4 to 4.8 Ma (using combined K-Ar and Rb-Sr age dates; Table 1). This sequence of eruptions culminated with the largest volume Real Grande Ignimbrite on the western flanks and the Cueva Negra Ignimbrite on the eastern flanks, which were interpreted as correlative deposits of the same eruptive episode.

Initial volume estimates of these deposits were based on several assumptions. Sparks et al. (1985) extrapolated the thickness (250 m) of ignimbrites belonging to the Toconquis Formation to uncharted areas north of the caldera. A combined volume of 400-500 km^3 for the whole formation was proposed based on mapped exposure, deposit thickness and the assumption that significant deposition occurred in the area now occupied by the modern caldera. This estimate was considered a minimum value, based on the inference that distal deposits ~80 km to the north of the caldera are correlative (Gonzalez 1984). The relative thickness of the Real Grande Ignimbrite suggested that it comprised two-thirds of the total Toconquis Formation volume (~500 km^3).

The volume of the Cerro Galán Ignimbrite (CGI) was estimated as about twice the volume of all the older ignimbrites combined, at over 1,000 km^3 (DRE) of combined intracaldera and outflow sheet material. Sparks et al. (1985) reported that most of the preserved resurgent dome consists of welded CGI. An intracaldera CGI volume of at least 450 km^3 (DRE) was estimated. The outflow area of the CGI was estimated by extrapolating the thickness and distal extent observed on the western flanks radially around the caldera. Using an area of 7,500 km^2, they calculated an outflow volume of ~280 km^3 (DRE). The average thickness and deposit density of the CGI was not reported, but using a typical, non-welded ignimbrite density of ~1,500 kg/m^3, a thickness of 62 m would yield this volume. In addition to the currently preserved deposit volumes, Sparks et al. (1985) estimated an additional volume of material lost to erosion and co-ignimbrite ash production approximately equal to the outflow volume, summing to a total in excess of 1,000 km^3.

Table 1 Previous age determinations on various sample from the Cerro Galán region (from Francis et al. 1983; Sparks et al. 1985)

Rock type or ignimbrite	Locality	Material sampled	Mineral	Age ±2σ (Ma) errors	Dating method	Source
Post caldera dome	Agaus Callentes		Biotite	2.10±0.28	K-Ar	Sparks et al. (1985)
CGI	Western flanks	Pumice	Biotite	2.72±0.15	K-Ar	Sparks et al. (1985)
CGI	Eastern flanks	Pumice	Biotite	2.57±0.16	K-Ar	Sparks et al. (1985)
CGI	Western flanks	Whole rock	Biotite	2.49±0.12	K-Ar	Francis et al. (1983)
CGI	Western flanks	Whole rock	Biotite	2.46±0.12	K-Ar	Francis et al. (1983)
CGI	Western flanks	Whole rock	Biotite	2.58±0.13	K-Ar	Sparks et al. (1985)
Intra caldera ignimbrite	Resurgent centre	Pumice	Biotite	3.04±0.15	K-Ar	Sparks et al. (1985)
Welded tuff	Resurgent centre	Whole rock	Biotite	3.65±0.45	K-Ar	Sparks et al. (1985)
Welded tuff	Resurgent centre	Whole rock	Biotite	3.80±0.49	K-Ar	Sparks et al. (1985)
Welded tuff	Resurgent centre	Whole rock	Sanidine	3.92±0.16	K-Ar	Sparks et al. (1985)
Pumice from ignimbrite	Leon Muerto valley	Pumice	Biotite	4.25±0.24	K-Ar	Sparks et al. (1985)
Welded tuff	Leon Muerto NE flanks	Whole rock	Biotite	4.19±0.26	K-Ar	Sparks et al. (1985)
Real Grande Lava	Caldera rim west flanks	Lava	Biotite	4.86±0.19	K-Ar	Sparks et al. (1985)
Real Grande Ignimbrite	Western flanks	Pumice	Biotite	5.14±0.29	K-Ar	Sparks et al. (1985)
Real Grande Ignimbrite	Western flanks	Pumice	Biotite	4.87±0.39	K-Ar	Francis et al. (1983)
Real Grande Ignimbrite	Western flanks	Pumice	Biotite	4.80±0.24	K-Ar	Francis et al. (1983)
Upper Merihuaca	Western flanks	Pumice	Biotite	5.14±0.21	K-Ar	Sparks et al. (1985)
Upper Merihuaca	Western flanks	Pumice	Biotite	5.38±0.26	K-Ar	Francis et al. (1983)
Lower Merihuaca	Western flanks	Pumice	Biotite	6.39±0.57	K-Ar	Sparks et al. (1985)
Old hornblende welded tuff	Eastern flanks	Whole rock	Biotite	15.83±0.44	K-Ar	Sparks et al. (1985)
Old hornblende welded tuff	Eastern flanks	Whole rock	Biotite	14.75±0.40	K-Ar	Sparks et al. (1985)
CGI pumice	Leon Muerto	Pumice	Bt, plag, sanidine, glass	2.03±0.07	Rb-Sr	Sparks et al. (1985)
Whole-rock welded tuff	Resurgent centre	Whole rock	Bt, plag, sanidine	2.39±0.15	Rb-Sr	Sparks et al. (1985)
Dacite lava	Real Grande lava	Lava	Bt, plag	4.00±0.22	Rb-Sr	Sparks et al. (1985)
Hornblendic welded tuff	Eastern flanks	Whole rock	Bt, plag	14.22±0.33	Rb-Sr	Sparks et al. (1985)
Amphibolite	SW calderarim		Hornblended	599.8±13	K-Ar	Sparks et al. (1985)
Follated Diorite	E caldera rim		Muscovite	417.0±9.8	K-Ar	Sparks et al. (1985)
?	Rim		Biotite	422.0±9.8	K-Ar	Sparks et al. (1985)
Granite	SW hot springs		Muscovite	347.0±8.2	K-Ar	Sparks et al. (1985)
Augen-gneiss	Colcha in caldera		Biotite	365.0±9	K-Ar	Sparks et al. (1985)

We reinterpret the stratigraphy and volume estimates of Sparks et al. (1985) based on comprehensive field-work, precise $^{40}Ar/^{39}Ar$ age determinations and new magnetostratigraphic data. Based on these data and detailed deposit maps and stratigraphic logs, we report a more detailed stratigraphy that includes newly distinguished ignimbrites; we produce a new geologic map of the Galán region; and we report better-constrained volume estimates

Methods

For clarification, the term 'Galán ignimbrites' refer to *all* the ignimbrites associated with this caldera, whereas the 'Cerro Galán Ignimbrite' (CGI) refers only to the largest, most recent ignimbrite, from the eruption that produced the modern caldera. The localities at Rio de Las Pitas, ~12 km from the western structural margin and Rio Pirica, ~10 km from the southwestern structural margin (see Fig. 2a, b for locations; Figs. 1, 2 in electronic supplementary material), were chosen to examine the stratigraphy in detail, as they contain the most complete sections of the older Toconquis Ignimbrites. The Cueva Negra Ignimbrite is the only pre-CGI ignimbrite not observed at these localities, as it is found exclusively on the eastern flanks (Fig. 2c). Samples for $^{40}Ar/^{39}Ar$ dating were selected from these three localities, with corresponding paleomagnetic analyses Lesti et al. (2011) performed on the same ignimbrites. We did not revisit all of the Sparks et al. (1985) localities, but covered a broader geographic area to understand the geographic distribution of deposits.

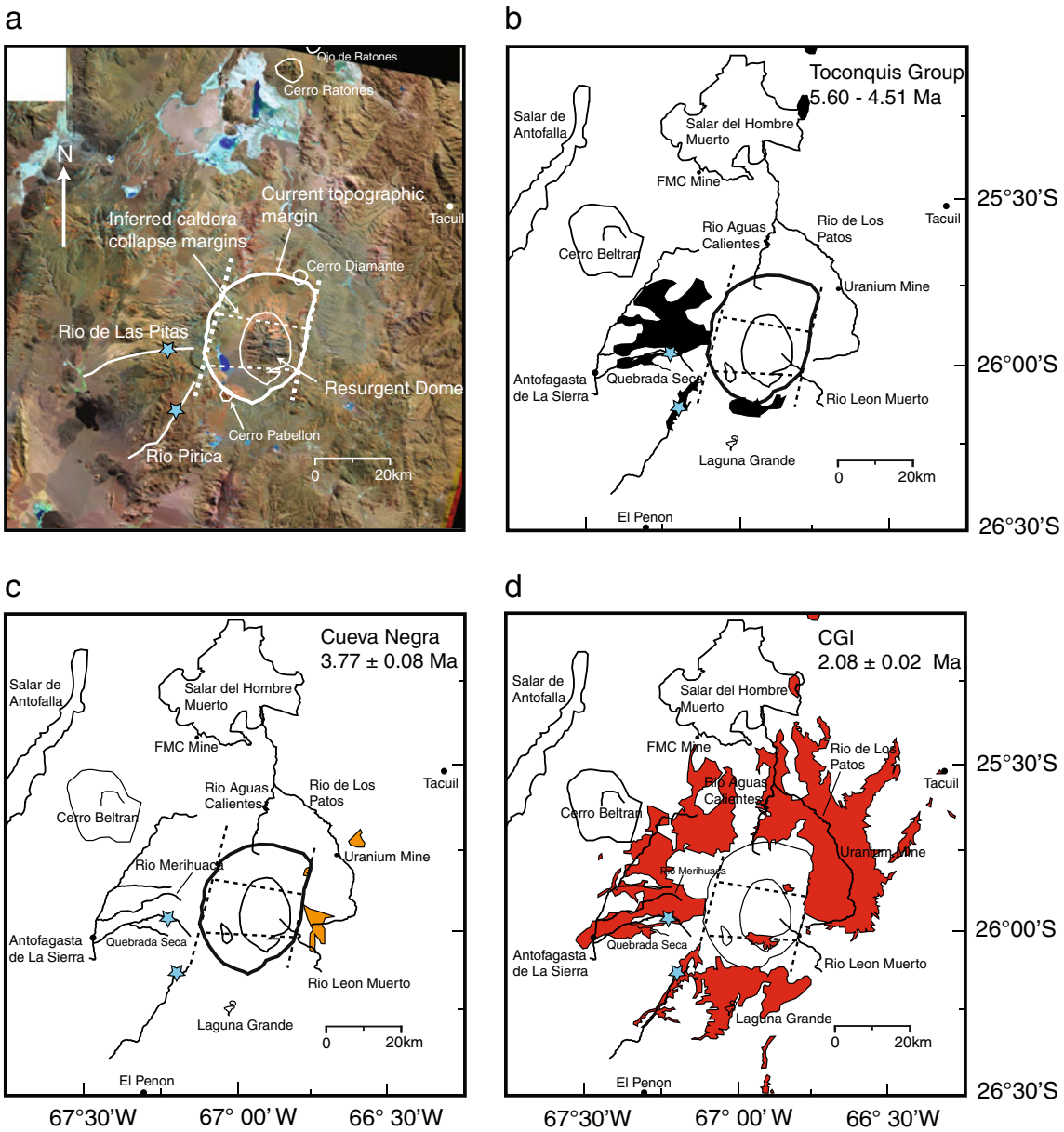

Fig. 2 **a** Landsat image of the Cerro Galán caldera. The star symbols refer to the two localities (Rio de Las Pitas and Rio Pirica) which show the best exposures of older ignimbrites along with the Cerro Galán Ignimbrite. **b–d** Ignimbrite deposit maps for **b** The Toconquis Group Ignimbrites, **c** The Cueva Negra Ignimbrite and **d** The Cerro Galán Ignimbrite (CGI)

$^{40}Ar/^{39}Ar$ geochronology

$^{40}Ar/^{39}Ar$ ages were determined by extracting biotite phenocrysts from juvenile clasts within each ignimbrite. Thin sections from these clasts were examined to check that biotite crystals showed no signs of alteration or breakdown. Biotite was selected because of its high abundance and presence in all ignimbrites. Sanidine was excluded from $^{40}Ar/^{39}Ar$ analyses due to its absence in the older Toconquis Ignimbrites (Folkes et al. 2011). Sample material was prepared by crushing and sieving the relevant samples, with heavy liquid separation used to isolate the density fraction relevant for biotite. Care was taken to select fresh, unaltered biotite without any adhering glass or ash from the ignimbrite matrix. At least 40 mg of material was then stacked into quartz vials and loaded in an irradiation tube before undergoing a 6 h irradiation at 1 MW at the Oregon State University (Corvallis) TRIGA research reactor. The Fish Canyon Tuff biotite standard was used (28.02± 0.16 Ma, Renne et al. 1998). Incremental heating $^{40}Ar/^{39}Ar$ age determinations were performed using a CO_2 laserprobe combined with a MAP-215/50 mass spectrometer at Oregon State University. Samples were heated in 50–100° C increments, from 400°C to fusion (6–13 steps, depending

on K-content). Incremental heating plateau ages and argon-isotope isochron ages were calculated as a weighted mean with $1/\sigma^2$ as the weighting factor (Taylor 1997) and a YORK2 least squares fit with correlated errors (York 1969) using the ArArCALC v2.2 software (Koppers 2002; Fig. 3).

Results

Revision of the Cerro Galán stratigraphy

The new biotite $^{40}Ar/^{39}Ar$ ages (calculated as weighted plateaus) are consistent with our stratigraphic framework (Table 2; Fig. 3). Figure 4a shows a generalized stratigraphic section through the Galán Ignimbrites (extracaldera) and their associated ages from the new biotite $^{40}Ar/^{39}Ar$ age determinations and magnetic polarity for each ignimbrite. The previous stratigraphy and K-Ar dates from Sparks et al. (1985) are shown for reference (Fig. 4b). We have retained many of the ignimbrite names introduced by Sparks et al. (1985). The new ages largely agree with those published by Francis et al. (1983) and Sparks et al. (1985) but there are some differences. This is most likely due to the wider range of analyzed material used by these previous authors, such as combined juvenile clast and matrix material analyses of biotite, plagioclase and glass (Table 1). $^{40}Ar/^{39}Ar$ dates are correlated with the magnetic polarities identified by Lesti et al. (2011), and these results are presented alongside the new biotite $^{40}Ar/^{39}Ar$ dates in Fig. 4c. The chronology of the magnetic polarity scale is taken from Cande and Kent (1995).

There is evidence to suggest that different minerals return slightly discordant ages. For example, Hora et al. (2011) have shown that biotite ages can exceed those of coeval sanidine in the same eruptive material by up to 500 kyr. This is confirmed for the CGI, for which the 2.56±0.05 Ma $^{40}Ar/^{39}Ar$ age from biotite crystals is 480 kyr older than the average 2.08±0.02 Ma $^{40}Ar/^{39}Ar$ age of sanidine crystals dated from the CGI outflow sheet by Kay et al. (2011). This younger age is consistent with the Rb-Sr age determinations from a combination of biotite, plagioclase and sanidine crystals for the CGI by Sparks et al. (1985). It is likely that the biotite $^{40}Ar/^{39}Ar$ ages of the older Cueva Negra and Toconquis Group Ignimbrites are also older than their 'true' eruption ages. However, the absence of sanidine in these older ignimbrites precludes calculation of their 'equivalent' sanidine ages. Furthermore, we cannot use a 480 kyr correction factor (the difference between biotite and sanidine ages for the CGI) for the whole stratigraphy, as the amount of offset between biotite and sanidine ages is not always consistent (Hora et al. 2011). However, our use of biotite throughout the $^{40}Ar/^{39}Ar$ age determinations yields an internally consistent system that can be used to assess both the repose periods between individual eruptions and the longevity of the magmatic system. The flat undisturbed age spectra and close fit of the data to inverse isochrons with an atmospheric $^{36}Ar/^{40}Ar_{(i)}$ component (Fig. 3) testify to the robustness and precision of the quoted biotite dates.

Toconquis ignimbrites

We have reclassified the Toconquis Formation of Sparks et al. (1985) as the Toconquis Group because it contains both the Merihuaca Formation (consisting of the Lower, Middle and Upper members that have very similar field characteristics and were erupted over a 110 kyr period; Table 2), and four additional ignimbrites. The oldest ignimbrite in the Toconquis Group is the Blanco Ignimbrite. The maximum exposed thickness of this ignimbrite is 7 m, although its true base is not observed. This ignimbrite is massive, and relatively pumice- (15%) and crystal-rich (20%). The large ash fraction makes the outcrop highly friable and susceptible to weathering. Unfortunately, we were unable to generate reliable biotite ages for the Blanco Ignimbrite because of extensive alteration where it is exposed at the Rio de Las Pitas section (Fig. 5). Paleomagnetic analyses of lithic clasts show this ignimbrite to have a normal polarity (Fig. 4a).

The base of the Lower Merihuaca Ignimbrite is marked by a 70 cm-thick sequence of alternating thin beds of ash-fall and surge layers. All of the Merihuaca Formation Ignimbrites (Lower, Middle and Upper members) are massive, pumice-rich (up to 40%), lithic-poor (<5%) and crystal-rich (25–30%). Juvenile clasts from the base of each ignimbrite yield biotite $^{40}Ar/^{39}Ar$ ages of 5.60±0.20 Ma for the Lower Merihuaca, 5.56±0.15 Ma for the Middle Merihuaca, and 5.49±0.11 Ma for the Upper Merihuaca Ignimbrite. The Middle Merihuaca Ignimbrite is underlain by a thin (<50 cm) fines-depleted surge deposit. The Middle and Upper members contain 1–3 m-thick pumice concentration zones (PCZ's) consisting of large pumice clasts up to 30 cm in diameter. The entire Merihuaca Formation is ~45 m thick at its thickest points at the Rio de Las Pitas section (~12 km from the western structural margin), where it is dominated by the Middle (25 m thick) and Upper (14 m thick) members. The Merihuaca Ignimbrites are absent >15 km from the western structural margin (Fig. 6). Lithic clasts in the Upper Merihuaca Ignimbrite preserve reverse polarity magnetization. The Middle and Lower Merihuaca Ignimbrites have normal polarities, which are not consistent with the polarity expected from their biotite $^{40}Ar/^{39}Ar$ dates (Fig. 4c), likely due to the aforementioned accuracy of using biotite in generating eruption ages. Using a combination of observed polarities, the chronology of the magnetic polarity scale calculated by

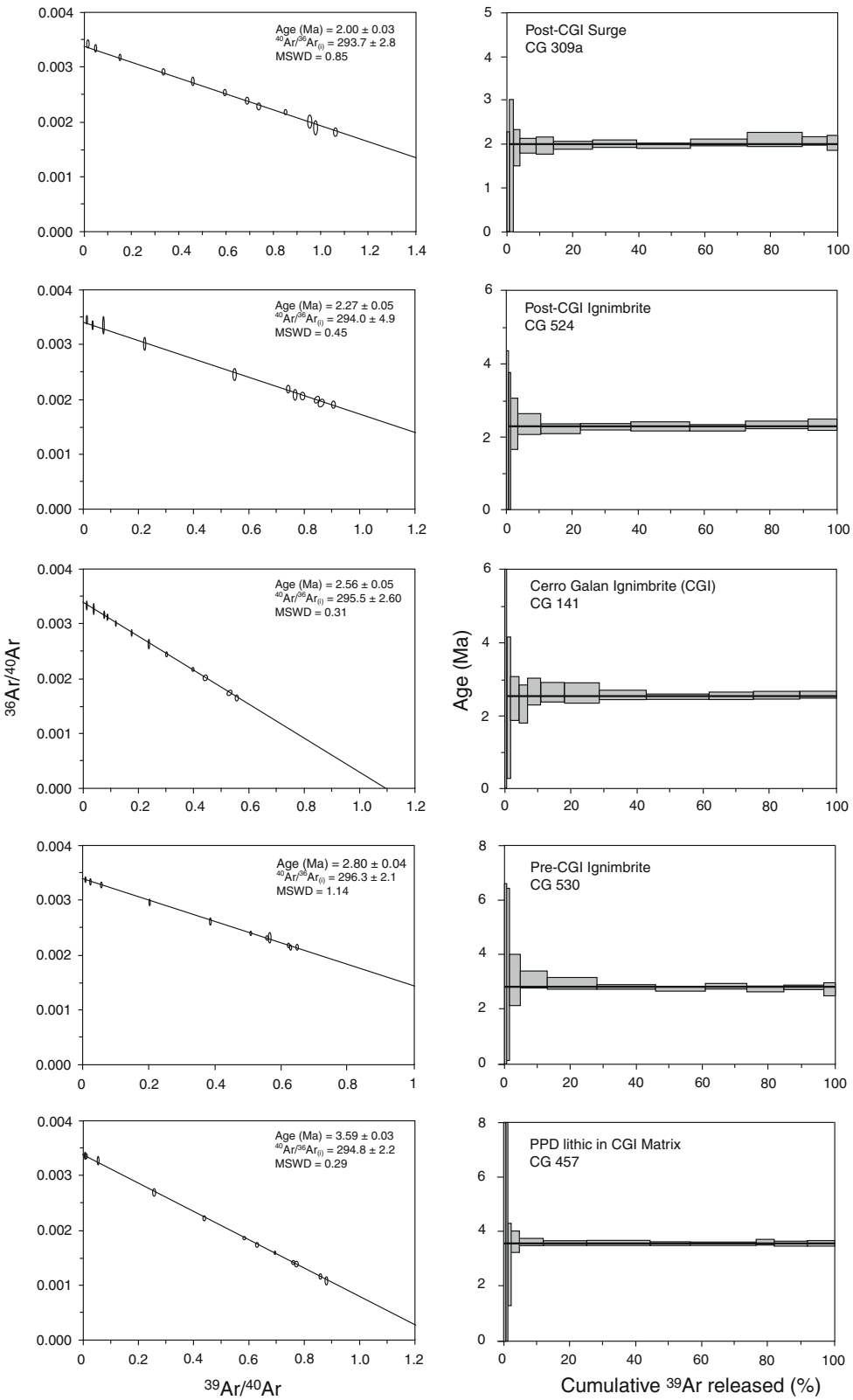

Fig. 3 Age spectra and inverse isochrons for samples at Cerro Galán. Biotite $^{40}Ar/^{39}Ar$ ages calculated using the weighted plateau function of the ArArCALC v2.2 software (Koppers 2002). 2 sigma errors are shown. All data points and steps for each experiment are shown. Grey boxes indicate accepted plateau steps; open boxes are excluded in the age calculations. The samples exhibit generally flat, undisturbed spectra except for CG 83, CG 91, CG 519, CG 227a, CG 112 and CG 486 which show disturbance in the low temperature steps. All samples (within error) show either an atmospheric or an elevated $^{40}Ar/^{36}Ar_i$ (trapped) component ($^{40}Ar/^{36}Ar$ >295.5±0.5), except for slightly lower values in CG 91 and CG 83

Fig. 3 (continued)

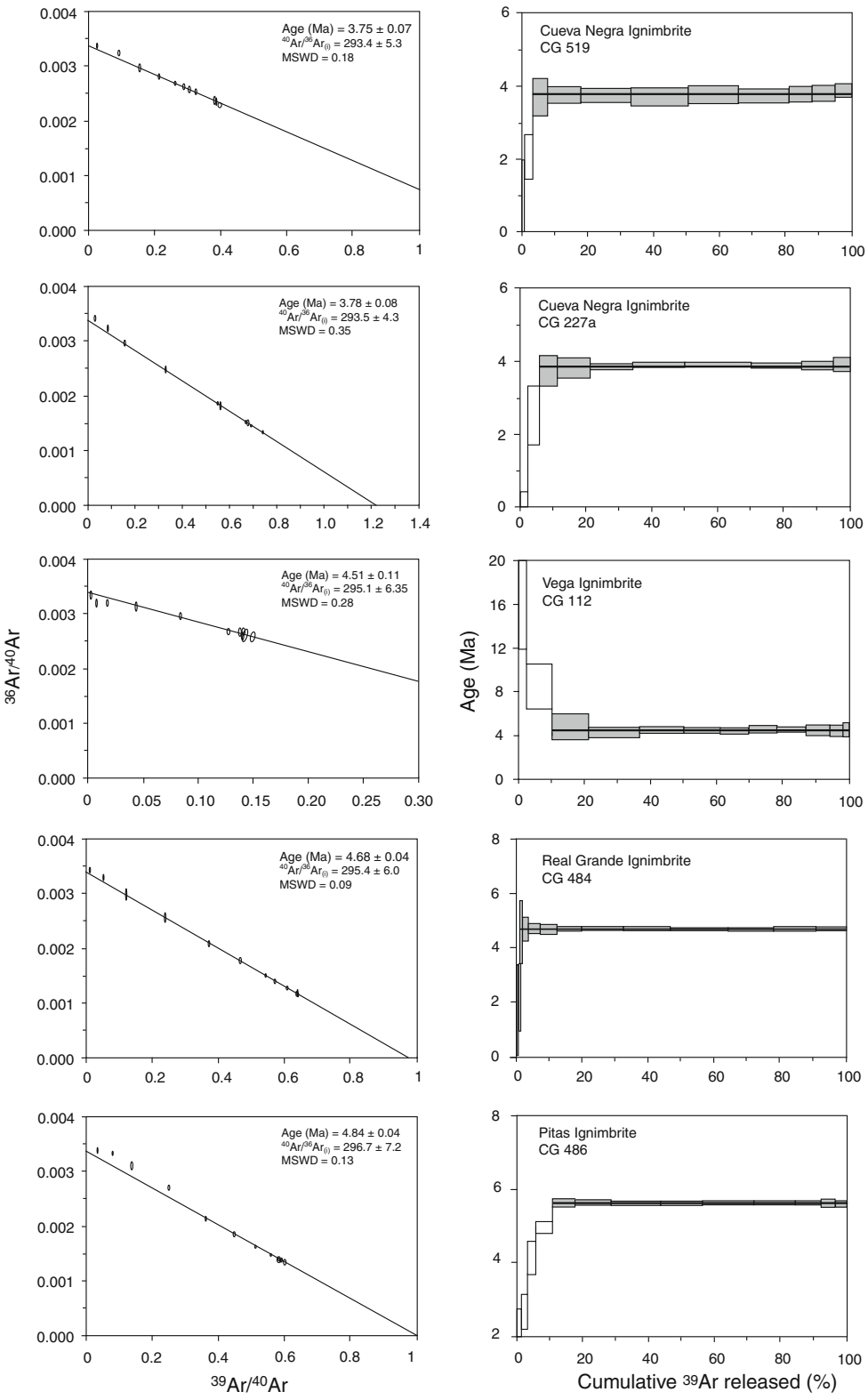

Fig. 3 (continued)

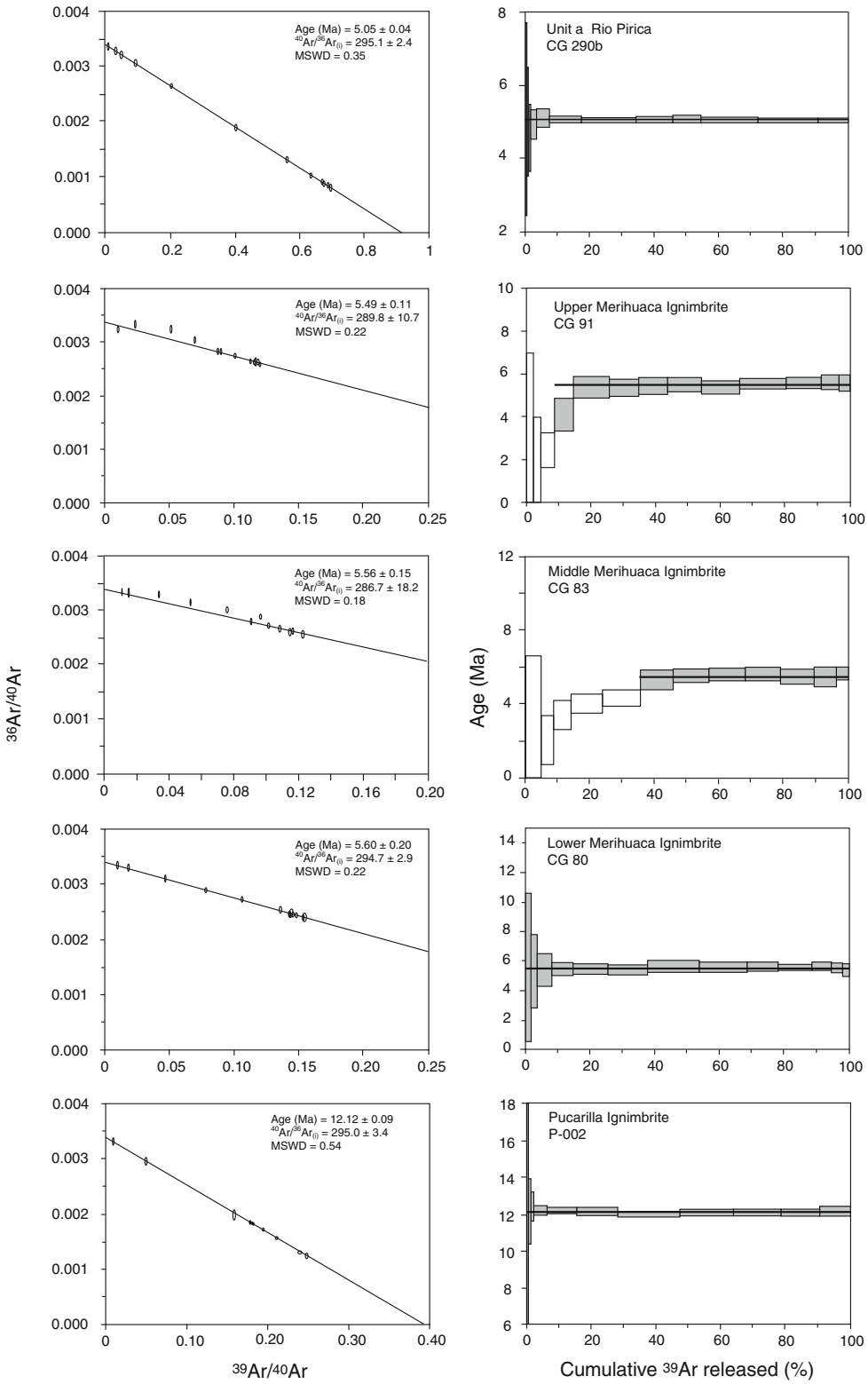

Table 2 New biotite 40Ar/39Ar dates for ignimbrites and other deposits in the Cerro Galán system

Ignimbrite or unit	Locality	Rock type	Co-ordinates (UTM)	Mineral	K/Ca	2σ	Plateau steps (°C)	40Ar/36Ar(i)	2σ	[a]Age + 2σ error (Ma)	Sample no.	[b]Polarity
Post-CGI Surge	Diamante surge platorm—proximal north	Single Pumice	0711237 7150983	Biotite	28.5	1.8	600–1400	293.7	2.8	2.00±0.03	CG 309	
Post-CGI Ignimbrite	Intracaldera—north	Single Pumice	0708329 7140423	Biotite	53.3	11.6	600–1400	293.9	4.9	2.27±0.05	CG 524	
Cerro Galan	Rio Merihuaca—proximal west	Single Pumice	0671280 7125619	Biotite	19.7	0.9	500–1400	295.4	2.6	2.56±0.05	CG 141	Reverse
Pre-CGI Ignimbrite	Intracaldera—south	Single Pumice	0711642 7116772	Biotite	4.1	0.2	500–1400	296.2	2.1	2.80±0.04	CG 530	
Cerro Galan	Eastern caldera—proximal	Lithic Clast in CGI	0719639 7129685	Biotite	16.7	0.8	500–1400	294.8	2,2	3.59±0.03	CG 457	
Cueva Negra	Eastern Caldera—proximal	Single Pumice	0718025 7138721	Biotite	14.3	0.5	850–1400	293.5	4.3	3.78±0.08	CG 227a	Reverse
Cueva Negra	Leon Muerto—proximal east	Single pumice	0718993 7121058	Biotite	1.6	0.05	700–1400	293.4	5.3	3.75±0.07	CG 519	Reverse
Vega	Rio de Las Pitas—proximal west	Single Pumice	0678932 7124869	Biotite	10.2	0.3	700–1400	295.1	6.4	4.51±0.11	CG 112	Reverse
Real Grande	Rio de Las Pitas—proximal west	Single Pumice	0678932 7124869	Biotite	20.8	0.7	700–1400	295.4	5.9	4.68±0.07	CG 484	Normal
Pitas	Rio de Las Pitas—proximal west	Single Pumice	0678981 7124972	Biotite	11.6	0.3	875–1400	296.7	7.2	4.84±0.04	CG 486	Normal
Basal unit, Pitas	Rio Pirica—proximal south-west	Single Pumice	0685959 7108171	Biotite	17.3	0.6	500–1400	295.1	2.4	5.05±0.04	CG 290b	
Upper Merihuaca	Rio de Las Pitas—proximal west	Single Pumice	0678932 7124869	Biotite	10.7	0.3	800–1400	289.9	10.7	5.49±0.11	CG 91	Reverse
Middle Merihuaca	Rio de Las Pitas—proximal west	Single Pumice	0678932 7124869	Biotite	12	0.4	975–1400	286.7	18.2	5.56±0.15	CG 83	Normal
Lower Merihuaca	Rio de Las Pitas—proximal west	Single Pumice	0678932 7124869	Biotite	12.5	0.4	500–1400	294.7	2.9	5.60±0.20	CG 80	Normal
Pucarilla Ignimbrite	East of the Galan caldera	Single Pumice	0767993 7131689	Biotite	8	0.3	500–1400	295	3.4	12.12±0.09	P-002	

[a] All ages calculated as weighted plateaus from biotite $^{40}Ar/^{39}Ar$ age determinations

[b] Polarity measurements by Lesti et al. (2011)

Cande and Kent (1995; based on sanidine $^{40}Ar/^{39}Ar$ ages) and our biotite $^{40}Ar/^{39}Ar$ ages, we can constrain the Merihuaca Formation Ignimbrites as follows: Lower and Middle Merihuaca—5.11±0.13 Ma (age range of the C3n.4n chron; Fig. 4c), Upper Merihuaca 4.94±0.05 Ma (Fig. 4c). These corrected ages are ~450 to 550 kyr younger than their respective biotite $^{40}Ar/^{39}Ar$ ages, similar to the difference between biotite and sanidine $^{40}Ar/^{39}Ar$ ages in the CGI.

The base of the overlying ignimbrite, here called the Pitas Ignimbrite, is marked by a laterally discontinuous layer (~8 m at its maximum thickness) with a high proportion of lithic clasts (up to 20%). Although the contact with the underlying Upper Merihuaca Ignimbrite is not observed, a juvenile clast from just above this lithic-rich horizon yielded a biotite $^{40}Ar/^{39}Ar$ age of 4.84±0.04 Ma. Paleomagnetic analyses of lithic clasts at this same stratigraphic level indicate normal magnetic polarity, confirming its distinction from the underlying reversely polarized Upper Merihuaca Ignimbrite. This ignimbrite is massive, pumice-rich (30%), lithic-poor (<5%) and contains at least three PCZ's with thicknesses similar to those in the Middle and Upper Merihuaca Ignimbrites. The Pitas Ignimbrite is much thicker (~60 m) at the Rio de Las Pitas section than the underlying ignimbrites, and the upper 18 m exhibits pervasive columnar jointing. This ignimbrite is absent at distances greater than 20 km from the western structural margin.

The base of the overlying Real Grande Ignimbrite is marked by a 50 cm-thick well-sorted pumice-rich deposit overlain by a light-colored, fines-depleted, weakly cross-stratified and laterally continuous basal portion of the ignimbrite. This basal layer forms a good marker horizon that is continuous for many kilometers from the western caldera margins and indicates a time break between the Pitas and Real Grande Ignimbrites. A juvenile clast from the base of the Real Grande Ignimbrite yields a biotite $^{40}Ar/^{39}Ar$ age of 4.68±0.07 Ma; lithic clasts show normal paleomagnetic polarity at the same stratigraphic level. The Real Grande Ignimbrite is the thickest ignimbrite in the Toconquis Group, ~120 m at its thickest points at the Rio de Las Pitas and Rio Pirica sections. This ignimbrite is absent >20 km from the western structural margin. The ignimbrite is massive, pumice-rich (up to 40%), crystal-rich (25–30%) and lithic-poor (<5%). There are at least five PCZ's up to 4 m thick, each containing individual pumice clasts up to 1 m in diameter. Isolated outcrops of the Real Grande ignimbrite occur to the north of Cerro Ratones (~70 km north of the structural margin), and are ~20 m thick at Ojo de Ratones, ~80 km north of the structural margin (Gonzalez 1984).

Immediately above the Real Grande Ignimbrite is a thin (2−3 m) pumice- (50%) and lithic-rich (25%) ignimbrite that has a biotite $^{40}Ar/^{39}Ar$ age of 4.51±0.11 Ma. The nature of the contact between this ignimbrite and the

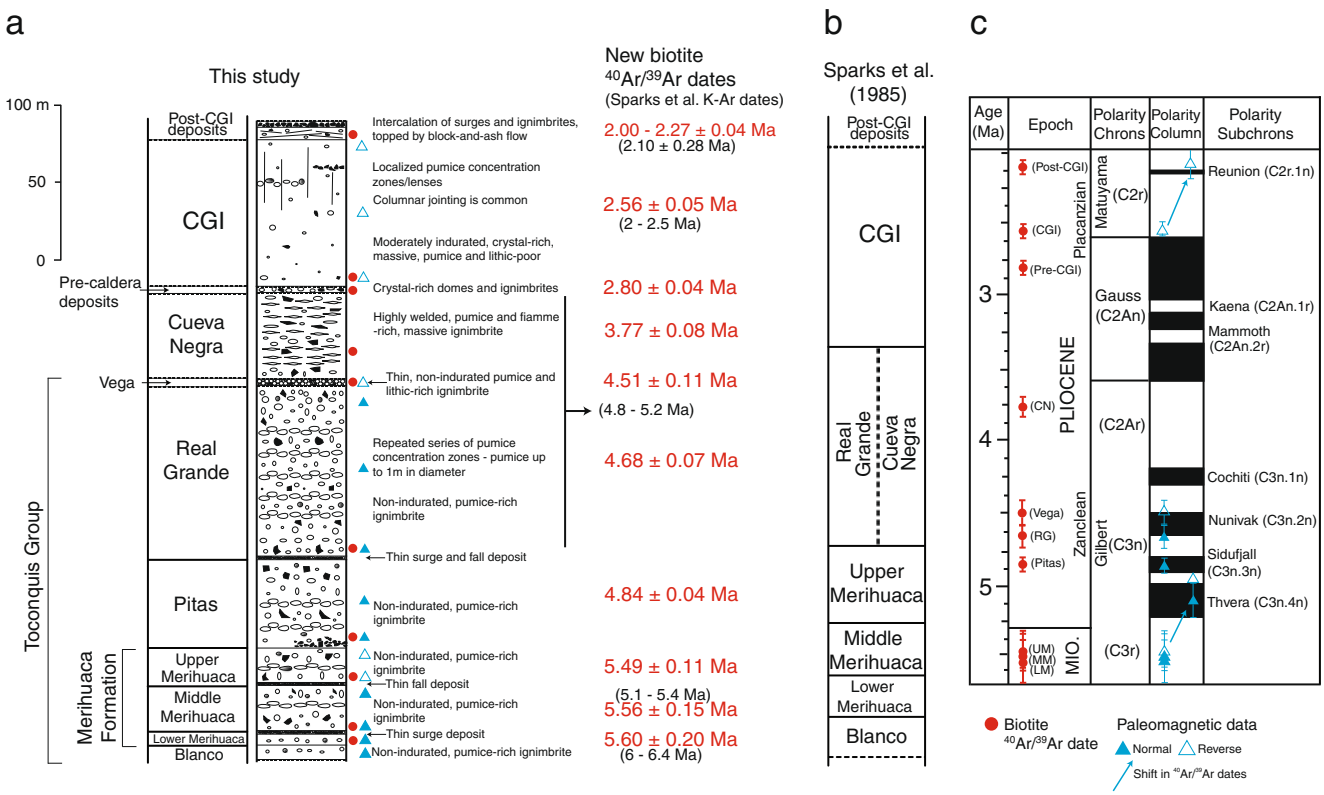

Fig. 4 The stratigraphy of the Galán Ignimbrites. **a** A representative sequence of the full stratigraphy associated with the Galán Ignimbrites. $^{40}Ar/^{39}Ar$ dates from biotite phenocrysts in juvenile clasts are shown along with previous K-Ar data (in parentheses) from Sparks et al. (1985). **b** The previous stratigraphy of Sparks et al. (1985) shown for comparison. **c** Magneto-stratigraphic scale (Lesti et al. 2011) showing the temporal positions of each ignimbrite. Note: red dots in **a** and **c** show the stratigraphic sampling level of $^{40}Ar/^{39}Ar$ samples (CN = Cueva Negra Ignimbrite; RG = Real Grande Ignimbrite; UM, MM, LM = Upper, Middle and Lower Merihuaca Ignimbrites, respectively). Blue triangles show stratigraphic sampling level of paleomagnetic lithic clast analyses—also shown on magneto-stratigraphic scale. The right-hand set of blue triangles in the polarity column in **c** indicates the shift of the CGI biotite $^{40}Ar/^{39}Ar$ age to the calculated sanidine $^{40}Ar/^{39}Ar$ age with one standard error bars shown (see text) and a shift in the Merihuaca Formation Ignimbrites biotite $^{40}Ar/^{39}Ar$ ages due to their observed polarities. The chronology of the magnetic polarity scale is taken from Cande and Kent (1995)

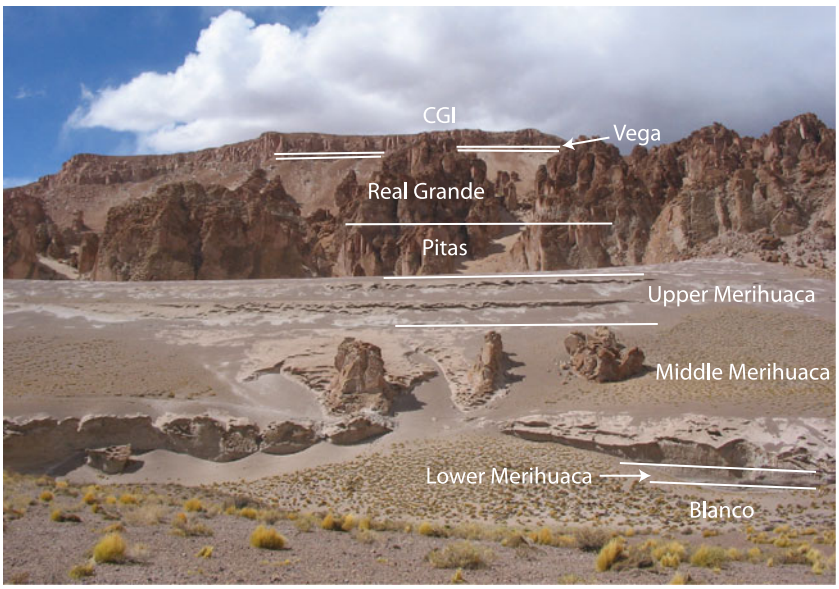

Fig. 5 Field photo of the Toconquis Group Ignimbrites capped by the CGI at Rio de Las Pitas, ~12 km west of the present structural margin. Photo taken facing north. Boundaries between ignimbrites are shown

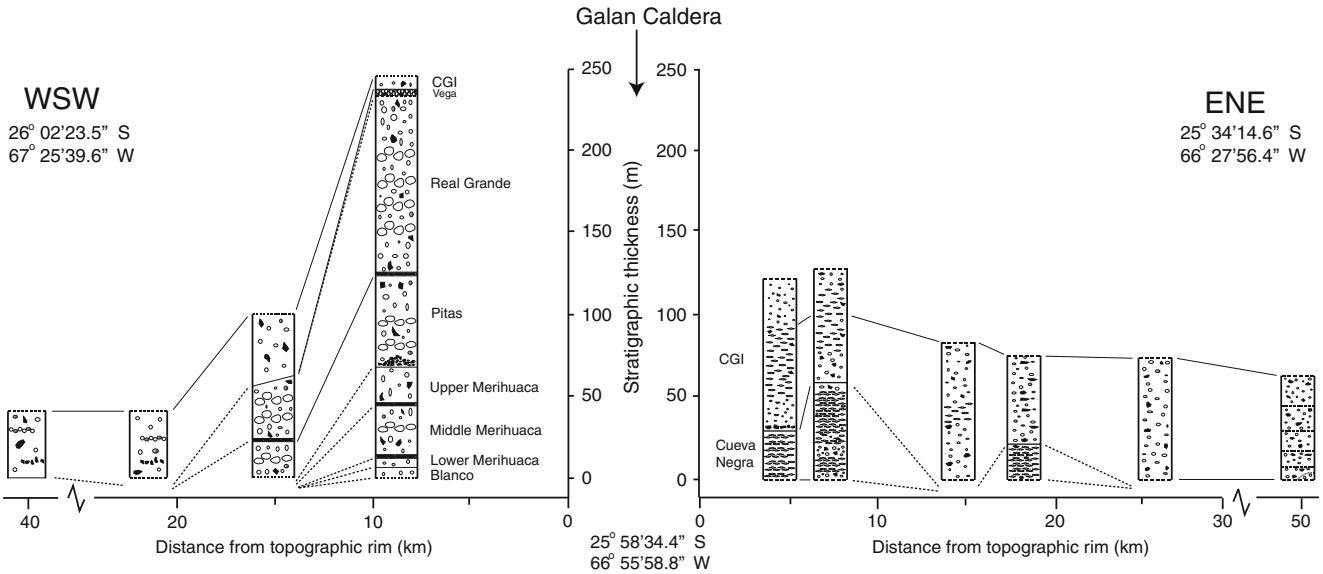

Fig. 6 Generalized stratigraphy of the ignimbrites on the eastern and western flanks of the Cerro Galán caldera

underlying Real Grande Ignimbrite is obscured by debris at the Rio de Las Pitas locality. Although the biotite $^{40}Ar/^{39}Ar$ age of the Real Grande Ignimbrite (4.68±0.07 Ma) is within error of this ignimbrite, there is a change in the magnetic polarity (from normal to reverse) between these two ignimbrites, indicating a time gap between deposition (Fig. 4c). Therefore, we consider this to be a new ignimbrite, which we have named the Vega Ignimbrite.

Finally, a single pumice clast was dated from the basal ignimbrite layer at the Rio Pirica section, returning a biotite $^{40}Ar/^{39}Ar$ age of 5.05±0.04 Ma. This age is close to that of the Pitas Ignimbrite dated in the Rio de Las Pitas section (4.84±0.04 Ma). However, this ignimbrite is only present beneath the Real Grande Ignimbrite at this locality and is more pumice-poor (~12%), crystal-poor (<20%) and lithic-poor (<3%) than the Pitas Ignimbrite at Rio de Las Pitas. This ignimbrite is only found in this locality; its spatial distribution is therefore unknown, but we suggest that it may represent a basal flow unit of the Pitas Ignimbrite.

Toconquis group summary

All ignimbrites belonging to the Toconquis Group (except the aforementioned lithic-rich base of the Pitas Ignimbrite) possess similar features. They are all crystal-rich (25–35%), pumice-rich (20–40%) and lithic poor (<5%). They are entirely non-welded, but indurated, and commonly contain 1–4 m-thick pumice concentration zones with individual pumice clasts up to 1 m in diameter. All the Toconquis Group Ignimbrites possess few internal structures or flow breaks, although some of the ignimbrites contain stratification due to sub-horizontal alignment of elongate pumice clasts. At the base of the Lower Merihuaca, Middle Merihuaca and Real Grande Ignimbrites are thin (<50 cm) fines-depleted layers consisting of intercalations of pyroclastic surges and/or airfall deposits. The thickness of these ignimbrites increases over time, culminating with the Real Grande Ignimbrite (Fig. 4a). All ignimbrites include three juvenile clast types: a dominant white, vesicular crystal-rich pumice variety, a grey or banded microvesicular, microcrystalline variety, and a much rarer, dense crystal-rich juvenile clast type. Two new ignimbrites; the Pitas and Vega Ignimbrites (biotite $^{40}Ar/^{39}Ar$ ages of 4.84±0.04 and 4.51±0.11 Ma, respectively); have been identified, updating the stratigraphy of Sparks et al. (1985). A new ignimbrite deposit map is shown in Fig. 2b and a generalized stratigraphy of the ignimbrites of the eastern and western caldera flanks is presented in Fig. 6. The Toconquis Group Ignimbrites (biotite $^{40}Ar/^{39}Ar$ ages of 5.60–4.51 Ma) are found primarily on the western and southwestern flanks, at a distance up to 25 km from the present-day structural margin.

Based on field descriptions, the Toconquis Ignimbrites were identified at widely distributed localities. The locality at Rio de Las Pitas contains about 240 m of continuous pyroclastic stratigraphy containing all of the Toconquis Ignimbrites (Fig. 5). The section at Rio Pirica contains the Real Grande and Pitas Ignimbrites. Isolated outcrops of the Toconquis Group Ignimbrites have been found at distal localities north of the caldera, east and north-east of Cerro Ratones (Fig. 2). At Ojo de Ratones (Fig. 2), we correlate the two basal ignimbrites with the Real Grande and Pitas Ignimbrites. A juvenile clast from the upper of these ignimbrites yielded a K-Ar age of 5.2±0.4 Ma (Gonzalez 1984), which is within error of our biotite $^{40}Ar/^{39}Ar$ age for the Real Grande Ignimbrite.

Cueva Negra ignimbrite

This ignimbrite is not seen in the section at Rio de Las Pitas and is found only on the eastern flanks of the present caldera margin up to the Rio de Los Patos valley (Figs. 2c and 6). The most proximal deposits of the Cueva Negra Ignimbrite are close to the present eastern structural margin of the caldera, suggesting that the source for this ignimbrite was along the eastern margins of the present caldera. The Cueva Negra Ignimbrite is characterized by a welded texture including fiammé (welding rank 4–5 of Quane and Russell 2005) throughout most of its stratigraphic thickness where observed near the current caldera margin. Where preserved, the base of this ignimbrite is non- to weakly-welded (welding rank 1–2) for ~6 m, above which welding increases upward over ~4 m, to a welding rank of 4–5 (Quane and Russell 2005), forming a black, eutaxitic texture. The ignimbrite is crystal-rich (25–30%), pumice-rich (15–25%) and lithic-poor (<5%), even in proximal localities. The maximum thickness is ~80 m at Rio Leon Muerto (average thickness is ~60 m) and it extends for at least 27 km to the east of the structural margin (Figs. 2c and 6). Two juvenile clasts from the base of the ignimbrite yield an average biotite $^{40}Ar/^{39}Ar$ age of 3.77±0.08 Ma (Fig. 4). Although Sparks et al. (1985) concluded that the Real Grande and Cueva Negra Ignimbrites were correlative, the new biotite $^{40}Ar/^{39}Ar$ ages indicate a period of quiescence between the Vega and Cueva Negra Ignimbrites of 0.74±0.14 Ma. Therefore, we distinguish the Cueva Negra Ignimbrite from the Toconquis Group Ignimbrites.

Cerro Galán Ignimbrite (CGI)

The youngest large-volume ignimbrite is the Cerro Galán Ignimbrite (CGI). This ignimbrite is extremely crystal-rich (35–50%), pumice-poor (<10%) and lithic-poor (<2%). Similar to the older Cueva Negra and Toconquis Group Ignimbrites, the CGI contains white, grey and dense, crystal-rich juvenile clasts. The CGI is massive throughout most of its extent; it commonly fills pre-existing topography as valley-ponded ignimbrite. Localized pumice-rich lenses (up to 1 m thick; pumice clasts up to 40 cm in diameter) are observed in medial to distal localities of the outflow sheet, radially around the caldera. Discrete, multiple flow units are evident only in distal deposits to the east of the caldera (near Tacuil; see Fig. 2d), where paleotopography strongly influenced flow behavior. The western CGI outflow sheet is thin in proximal areas (~20 m at Rio de Las Pitas) and thickens to ~40 m at distances >40 km from the caldera structural margin, as described by Sparks et al. (1985). The most distal currently preserved extent of the CGI is north of Cerro Ratones, ~80 km to the north of the structural margin at Ojo de Ratones (Fig. 2a).

A single juvenile clast at the base of this ignimbrite (at the Rio de Las Pitas locality) yields a biotite $^{40}Ar/^{39}Ar$ age of 2.56±0.05 Ma; lithic clasts at the same stratigraphic level possess a reverse polarity (Fig. 4c). Gonzalez (1984) reports a K-Ar age of 2.4±0.1 Ma for the upper 24 m-thick unit at Ojo de Ratones, confirming the interpretation of distal-most CGI north of the caldera. As mentioned above, our biotite age is 0.48 Ma older than the 2.08±0.02 Ma age calculated from average sanidine $^{40}Ar/^{39}Ar$ ages by Kay et al. (2011). An eruption age of 2.08±0.02 Ma is consistent with reverse polarity lithics (Fig. 4) and is our preferred interpretation of the CGI eruption age.

Areal extent of the Galán Ignimbrites

Initial studies by Francis et al. (1983) and Sparks et al. (1985) estimated the CGI to be distributed 100 km, and the Toconquis Group Ignimbrites to be distributed 30 km, in all directions from the caldera 'rim'. This estimate was based on limited radial field coverage combined with inferences from satellite images. We have attempted to improve constraints on areal distribution of all the ignimbrites by using several localities (especially in distal areas) around the caldera to produce a new geologic map (Fig. 7). To infer the areal extent of ignimbrites, we have used maximum runout distances from the present-day structural margin (compared with distances from the caldera 'topographic' rim as quoted by Sparks et al. 1985). We find evidence of the Toconquis Group Ignimbrites up to 25 km from the structural margin on the southwestern and western flanks; the Real Grande and Pitas Ignimbrites are also found at Ojo de Ratones, a distal outcrop ~80 km to the north of the structural margin (Figs. 2b and 7). The locality at Rio Pirica was also shown to comprise at least two ignimbrites in the Toconquis Group, extending their areal distributions. The Cueva Negra Ignimbrite is found only to the east of the caldera, up to 27 km from the structural margin (Figs. 2c and 7). Our field constraints increase the estimated current areal extent of the Toconquis Group Ignimbrites to ~220–420 km^2 whereas the Cueva Negra Ignimbrite occupies an area of ~50 km^2 (Table 3).

Our mapping suggests the CGI distribution reported by Francis et al. (1983) and Sparks et al. (1985) is an overestimate; we find that the currently preserved extent of the CGI is only 40 km from the structural margins, except to the east and north of the caldera (Figs. 2d and 7). CGI is preserved to the east of the caldera at Tacuil (~50 km from the structural margin), and to the north of the caldera at Ojo de Ratones (~80 km from the structural margin). Based on their distribution estimates, Sparks et al. (1985) reported that the CGI had an outflow sheet area of ~7,500 km^2, but our calculations show that the currently preserved extent is closer to 2,400 km^2. Naturally, this reflects only the

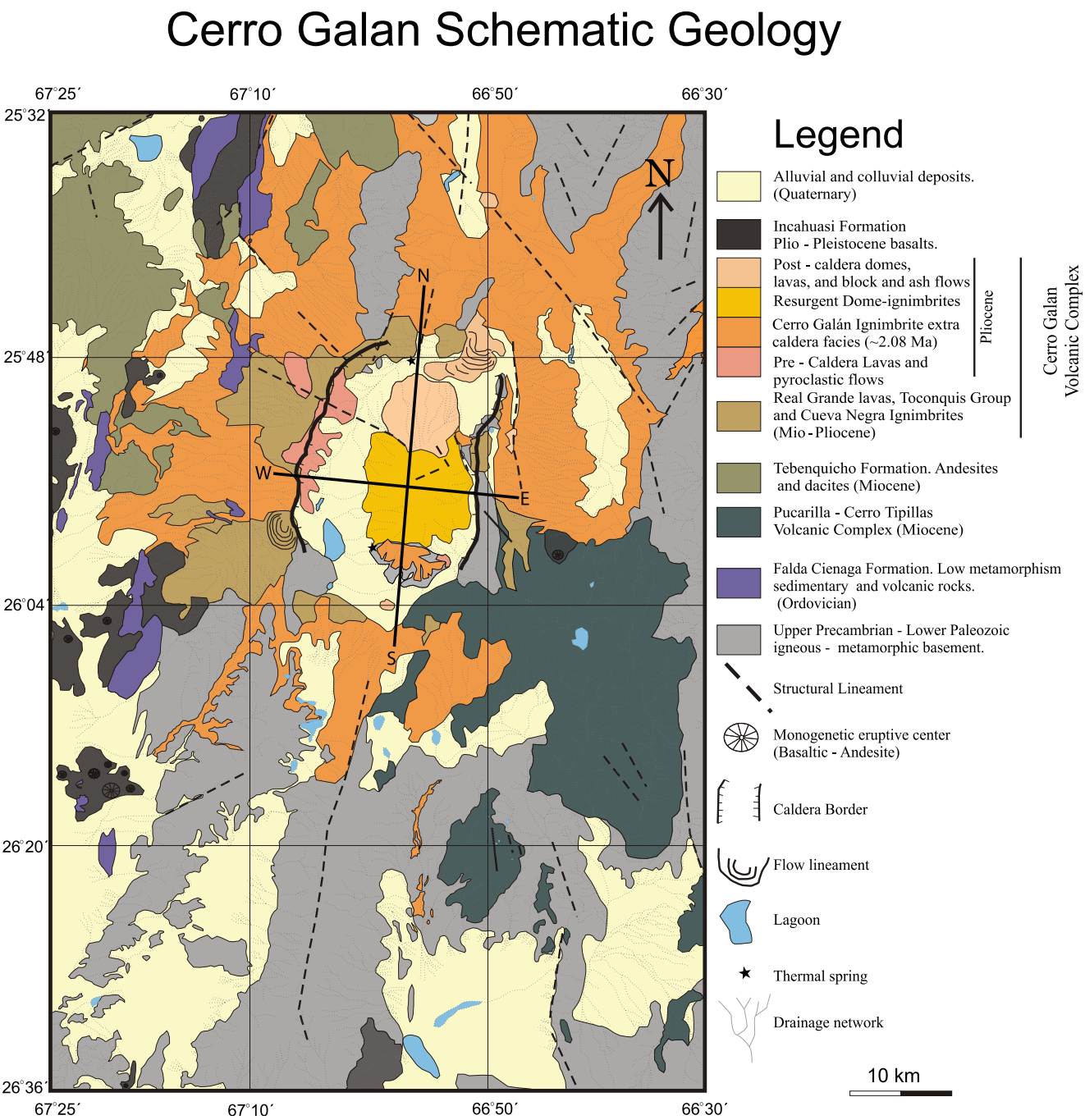

Fig. 7 Geologic map of the Cerro Galán caldera and surrounding region

preserved extent of the ignimbrite; a number of correction factors are required to estimate the original areal extent and bulk outflow sheet volume, and will be addressed later.

Pre- and post-caldera deposits

Many small-volume volcanic deposits within the present-day caldera pre-date the CGI, and many were found close to the southern and southwestern structural margins of the caldera (Fig. 7). These deposits mainly consist of fragmented lava domes with large (up to 2 m in diameter) brecciated and variably vesiculated juvenile blocks that are weakly flow banded (some outcrops are more coherent with little brecciation). We interpret these deposits to be a series of block-and-ash flow deposits (BAF's). There are also isolated deposits in this area that are crystal-rich (up to 40%), juvenile clast-rich (up to 40%) and lithic-rich (up to 20%). Juvenile clasts in these are more vesicular than those in the BAF's described above; we interpret these to be proximal ignimbrites deposited from high particle-

Table 3 New volume estimates for the Galán Ignimbrites

Ignimbrite (Biotite $^{40}Ar/^{39}Ar$ Age (Ma))	[a]Present outflow sheet area (km^2)	Average thickness (km)	Exposed volume (Ev (km^3))	[b]Factor A (Missing Outcrop)	Error	[c]Factor B (Co-ig. ash) ±0.25	[d]Factor C (Erosion) ±0.25	Ouflow sheet volume (bulk) (Ov (km^3) = Ev*A*B*C	[e]Intracaldera Fill volume (bulk (Iv (km^3))	Total bulk volume (Tv (km^3)) = Ov + Iv	[f]Total volume (DRE) (km^3) = (Ov*Od) + (Iv*0.98)	Error range (km^3)
CGI (2.56±0.05)	2400	0.045	108	1.5	±0.5	1.5	2	486	315	801	630	460–860
Cueva Negra (3.77±0.08)	50	0.060	3	4	±1	1.5	2	36	23	59	50	40–60
Real Grande (4.68±0.07)	420	0.090	38	2.75	±1	1.5	2	312	202	514	390	300–560
Pitas (4.84±0.04)	420	0.060	25	2.75	±1	1.5	1.5	156	101	257	190	150–290
Upper Merihuaca (5.49±0.11)	280	0.014	4	1.75	±0.5	1.5	1.5	15	10	25	20	15–30
Middle Merihuaca (5.56±0.15)	280	0.025	7	1.75	±0.5	1.5	1.5	28	18	45	35	30–50
Lower Merihuaca (5.60±0.20)	280	0.006	2	1.75	±0.5	1.5	1.5	7	4	11	8	7–11
Blanco	220	0.007	2	1.75	±0.5	1.5	1.5	6	4	10	8	5–10

[a] Present area of outflow sheet calculated by mapping in ArcGIS

[b] Factor A = missing preserved outcrop—connected from maps (see text)

[c] Factor B = co-ignimbrite ash. See text for explanation

[d] Factor C = missing outcrop—from erosion

[e] Intracaldera volume estimated for the CGI=315 km^3. Intracaldera volume for older ignimbrites assumed to be same proportion as for the CGI

[f] Magma density (water-free)=2450 kg/m^3 (Folkes et al. 2011). Intracaldera ignimbrite assumed to have a density of 2400 kg/m^3. CGI outflow ignimbrite density (Od)=1600 kg/m^3; Cueva Negra ignimbrite assumed density (Od)=2000 kg/m^3; Toconquis Group ignimbrite density (Od)=1500 kg/m^3

concentration pyroclastic flows. These ignimbrite deposits contain extremely large quartz, plagioclase and biotite phenocrysts (up to 15 mm in diameter) and pumice clasts up to 30 cm in diameter. A pumice clast from one of these deposits yields a biotite $^{40}Ar/^{39}Ar$ age of 2.80±0.04 Ma (Table 2, Fig. 4c), pre-dating the CGI $^{40}Ar/^{39}Ar$ biotite age by 0.24 Myr. In addition, Kay et al. (2011) report a sanidine $^{40}Ar/^{39}Ar$ age of 2.126±0.017 Ma for a sample locality that is close to our observed small-volume ignimbrite deposits on the southwestern structural margins of the caldera, pre-dating the CGI $^{40}Ar/^{39}Ar$ sanidine age by ~0.05 Myr.

Other evidence exists for periodic silicic dome construction and destruction. A large (8 cm in diameter) plagioclase-phyric dacite (PPD) lithic fragment contained within proximal CGI deposits on the eastern flanks of the caldera (CG 457) yields a biotite $^{40}Ar/^{39}Ar$ age of 3.59±0.03 Ma (Table 2). This is ~1 Myr older than the CGI biotite $^{40}Ar/^{39}Ar$ age and could represent lava-dome-building activity related to and post-dating the eruption of the Cueva Negra Ignimbrite (3.77±0.08 Ma biotite $^{40}Ar/^{39}Ar$ age).

Post-CGI deposits are found on the northern margins of the resurgent dome and in proximal areas to the north and east of the present-day caldera (Fig. 7). On the northern margins of the resurgent dome are a series of dense pumice-rich (up to 16%) and crystal-rich (40%) coarse ignimbrite or BAF deposits. The contact between these deposits and the underlying CGI is not seen. A juvenile clast was sampled from the base of a dense pyroclastic flow deposit and yielded a biotite $^{40}Ar/^{39}Ar$ age of 2.27±0.05 Ma (Table 2, Fig. 4c), post-dating the CGI biotite $^{40}Ar/^{39}Ar$ age by ~0.29 Myr.

The upper contact of the CGI is rarely preserved in any of the studied outcrops. However, it is observed ~20 km north of the structural margin to the west of Cerro Diamante (and northeast of the caldera ~5 km northwest of the uranium mine; Fig. 2). Immediately overlying the CGI to the north and northeast of the caldera are a series of alternating low-angle cross-bedded surge deposits and thin (<50 cm) ignimbrites (Fig. 3 in electronic supplementary material). A pumice clast from one of these ignimbrites yields a biotite $^{40}Ar/^{39}Ar$ age of 2.00±0.03 Ma (Table 2, Fig. 4c), post-dating the CGI biotite $^{40}Ar/^{39}Ar$ age by 0.56 Myr. This is the youngest age obtained for post-caldera volcanism associated with the present Cerro Galán caldera, and indicates a long-lived magmatic system from 5.6 to 2 Ma. Above these surge and thin ignimbrite layers is a block and ash-flow deposit at least 2 m in thickness (the upper contact is not seen), suggesting that post-caldera activity could have continued after 2 Ma. Furthermore, on the eastern topographic rim of the caldera, another BAF deposit up to 3 m thick locally (5×0.5 km in area) blankets the CGI. The combination of field relationships, biotite $^{40}Ar/^{39}Ar$ ages of small volume deposits, and dated lithic clasts within the CGI support punctuated small eruptions, in addition to large caldera-forming events throughout the eruptive history of Cerro Galán.

Summary of the Cerro Galán stratigraphy

Key differences between the previous stratigraphy constructed by Sparks et al. (1985) and this study include the following:

- We redifine the oldest group of ignimbrites as the Toconquis Group, which includes the Blanco Ignimbrite, the Merihuaca Formation Ignimbrites (comprising the Lower, Middle and Upper members), the Pitas Ignimbrite, the Real Grande Ignimbrite and the Vega Ignimbrite. Based on fieldwork and biotite $^{40}Ar/^{39}Ar$ ages, we have identified two new ignimbrites in the Toconquis Group. The Pitas Ignimbrite (4.84±0.04 Ma) was erupted after the Upper Merihuaca Ignimbrite (5.49±0.11 Ma) and before the Real Grande Ignimbrite (4.68±0.07 Ma). This agrees with the new work of Lesti et al. (2011), which documents a polarity reversal between the Upper Merihuaca and Pitas Ignimbrites (Fig. 4c). A thin (~2 m) newly-identified ignimbrite below the CGI coincides with another change in polarity from the Real Grande Ignimbrite (Fig. 4c). We have named this new ignimbrite the Vega Ignimbrite, with a biotite $^{40}Ar/^{39}Ar$ age of 4.51±0.11 Ma.
- The known extents of the Blanco, Lower, Middle and Upper Merihuaca Ignimbrites have been extended. We have found new localities (along Rio Pirica) to the southwest of the caldera and in the southern caldera wall that expose outcrops of the Pitas and Real Grande Ignimbrites with a comparable thickness and distribution to those documented in Vega Real Grande (Rio de Las Pitas; Fig. 2) by Sparks et al. (1985). Isolated outcrops of Real Grande and Pitas Ignimbrites occur to the north of the caldera, at Ojo de Ratones, ~80 km north of the structural margin (Figs. 2 and 7). This increases the outflow sheet volume estimates of the older Toconquis Group Ignimbrites.
- The Cueva Negra Ignimbrite was previously thought to have erupted concurrently with the Real Grande Ignimbrite, forming its eastern counterpart (Sparks et al. 1985). New biotite $^{40}Ar/^{39}Ar$ ages show, however, that the Cueva Negra Ignimbrite is a discrete unit erupted at 3.77±0.08 Ma, ~0.9 Myr after the Real Grande Ignimbrite (Fig. 4c). We now place this ignimbrite between the Toconquis Group Ignimbrites and the CGI.
- The known preserved extent of the CGI has been reduced based on our field observations. We show that the runout of the CGI extends 40 km in all directions

from the inferred structural margin (Figs. 2d and 7), although the maximum distal extent currently preserved is found at Ojo de Ratones, ~80 km from the structural margin. This has led to a reduction of the known preserved areal extent of the CGI compared with Sparks et al. (1985) to a new figure of 2,400 km^2.

Cerro Galán Caldera

Here, we present a revised interpretation of the elliptical 35×20 km Cerro Galán 'caldera' based on new mapping and satellite-image analysis. We broadly concur with Sparks et al. (1985) and Chernicoff et al. (2002) regarding the importance of regional faults in bounding the caldera, but our new mapping leads us to a different conclusion from the original idea of the entire depression being the result of the 'foundering of a coherent cauldron block' to form the 'caldera' during the climactic eruption of the Cerro Galán Ignimbrite. We believe that the Cerro Galán caldera is a smaller trapdoor collapse that occupies only the central part of the caldera as previously defined. Our assertions are based on a re-examination of the topographic margins of the Cerro Galán depression and investigation of the southern and northern parts of the resurgent dome.

Topographic and structural margins

Francis and Baker (1978) and Sparks et al. (1985) identified that the broadly elliptical depression of the Cerro Galán caldera is topographically bounded by N-S faults that extend through basement on the eastern and western caldera margins. Current topographic margins lie outside of the original structural boundaries due to erosion and mass wasting of the caldera walls (cf. Smith and Bailey 1966; Lipman 1997).

We investigated the topographic margins of the Cerro Galán caldera to better understand collapse history. Based on field mapping and examination of the stratigraphy, supplemented by examination of remote images and a 30 m resolution digital elevation model constructed from ASTER data, we address the nature of these margins and their relationship to the original caldera-bounding faults. We would expect the erosional remnants of caldera collapse scarps to form dissected ignimbrite and/or basement cliffs. Along the southern, northern, and eastern topographic margins, this is not the case; only along the western margin are steep ignimbritic and basement cliffs present.

The southern topographic margin (Fig. 8) consists of an 80 m high cliff of the Pitas, Real Grande and Cerro Galán Ignimbrites, which drape the pre-existing topography of Cerro Pabellon. Here, the basal ignimbrites ramp up the topography, away from the caldera, and large pumice lenses in the lowermost Pitas Ignimbrite clearly mimic the pre-existing slope on the northern side (toward the caldera). The three ignimbrites are therefore outflow facies of the respective eruptions, overtopping preexisting topography. The topographic expression of the southern margin clearly lies outside the original structural margin, but based on field evidence it is further outside the topographic margin than simple mass wasting would produce. Therefore, the Pitas, Real Grande and Cerro Galán Ignimbrites at this locality are inferred to be outflow ignimbrites.

The elevated northern rim of the topographic margin is an older volcanic massif now topped by the young Cerro Diamante dome (Fig. 9c). Here, the CGI flowed through a gap between the preexisting volcanic high of Cerro Diamante on the east and the Paleozoic basement block on the west, outside the original structural margin and vent location (Fig. 7). The site of the gap is now occupied by the hydrothermal springs and tufa deposits of Aguas Calientes, perhaps aligned with preexisting faults. There is no evidence for a steep fault scarp or the eroded remnant of such a scarp. Evidence for an original structural margin that accommodated major caldera collapse is therefore not present along the original northern topographic margin as defined by Sparks et al. (1985).

The eastern margin of the caldera is defined by a broad shallowly W-dipping slope that merges with the central part of the resurgent dome. This association led Sparks et al. (1985) to suggest that resurgence occurred by magma rise along the eastern bounding faults of the Cerro Galán caldera. Our mapping shows that the eastern flank of the depression consists of steeply dipping Paleozoic basement, as recognized by Sparks et al. (1985), but there is no clear evidence for a caldera-bounding fault. Instead, our observations suggest that the basement consists of steeply dipping foliated diorites, mica schists and amphibolites. This entire block is tilted westward in a broad monocline that is hinged at the drainage divide at 5,200 m (Fig. 9b). The southernmost expression of this margin is an inaccessible complex of ignimbrite and lava domes that are overlain by the CGI outflow, which we map on the eastern and southern flanks.

The western margin is a true topographic margin produced by erosion and mass wasting of the original structural margin. This margin follows a major N-S bounding fault and clearly truncates older volcanic structures, including the Toconquis massif in the north and the andesitic dome in the south that is probably related to the Real Grande massif, which lies just to the west (Fig. 9). Both the Toconquis center and the andesitic dome that formed along this bounding fault pre-date the CGI eruption. The upper 400 m of this 600 m high cliff clearly exposes basement topped by the early Toconquis Ignimbrites and

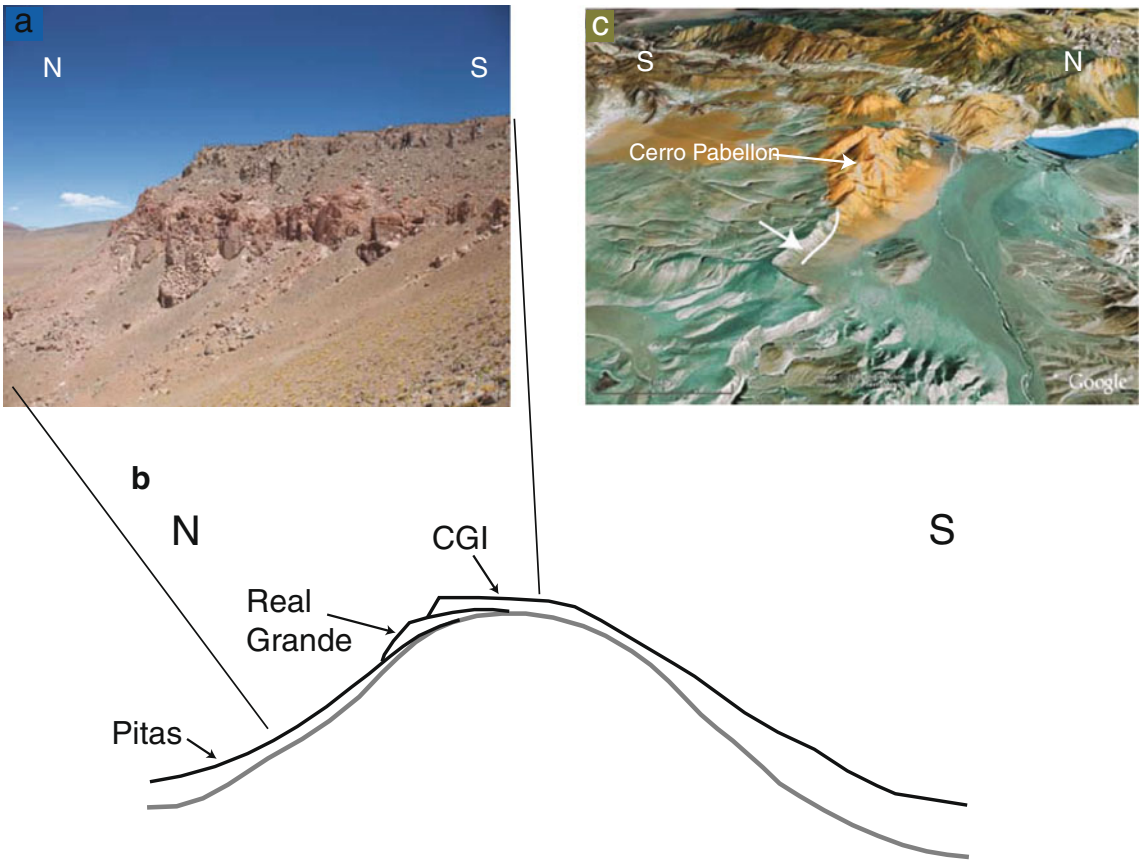

Fig. 8 **a** Southern margin of the Cerro Galán depression showing the pre-existing topography being draped by the CGI and Toconquis Ignimbrites. The former is just a thin smear at the top of the stratigraphic sequence (**b**). **c** Google Earth© perspective image (resolution ~30 m) of the Galán caldera showing the details of the southern margin. Lower arrow points to location of the sections in **a** and **b**

lavas, whereas the lowermost 200 m is covered in talus (Fig. 9). Sparks et al (1985) report ages of ~420 and 350 Ma from basement lithologies collected from this western 'wall'.

We conclude from these new observations that the topographic expression of the Cerro Galán caldera does not mimic the original collapse margin. The topographic highs bounding the caldera depression to the east, south and north are formed by pre-existing topography. Further evidence for major intracaldera collapse boundaries is found within the central, partially resurgent dome.

Resurgent dome

We agree with the interpretation of Sparks et al (1985) that most of the resurgent dome of Cerro Galán itself consists of CGI. However, it is now clear that the southernmost and northernmost parts of the dome contain little CGI or Toconquis Ignimbrites (Figs. 7 and 9). The southern portion of the resurgent dome and the hydrothermal area on its south-western margin consist of Paleozoic basement capped by a relatively thin veneer (20–30 m) of outflow CGI (Figs. 7 and 10). The basement-dominated southern region of the dome is separated from the central ignimbrite-dominated portion of the dome by an E-W-trending fault (Fig. 11), as recognized by Sparks et al. (1985). These new observations of the resurgent dome are also shown on the updated geologic map and cross sections (Figs. 7 and 9).

The northern moat of the Cerro Galán depression contains a fan of volcaniclastic deposits (small ignimbrites and block and ash flow deposits) that extend from older Diamante lavas in the north to the northern portion of the central ignimbrite-dominated portion of the resurgent dome (Fig. 9). Sparks et al (1985) identified this region as a post-CGI complex that erupted along a fault bounding the

Fig. 9 Geologic cross sections **a** N-S and **b** E-W across the Cerro Galán depression. Vertical exaggeration is ×5. Profiles were generated from a 30 m-DEM generated image using ASTER data. Interpreted floor geometry shown as piecemeal blocks. Post-collapse resurgent geometry of blocks is compared with immediate post collapse geometry shown in red. Approximate location of major caldera bounding faults is shown. **c** Perspective view produced with ASTER data draped over the ASTER-30 m DEM showing the location of main features at Cerro Galán. Location of the cross sections is shown by the heavy black dashed lines. A is the southern basement-dominated portion of the resurgent dome, and B is the post resurgent dome and volcaniclastic apron complex on the north.

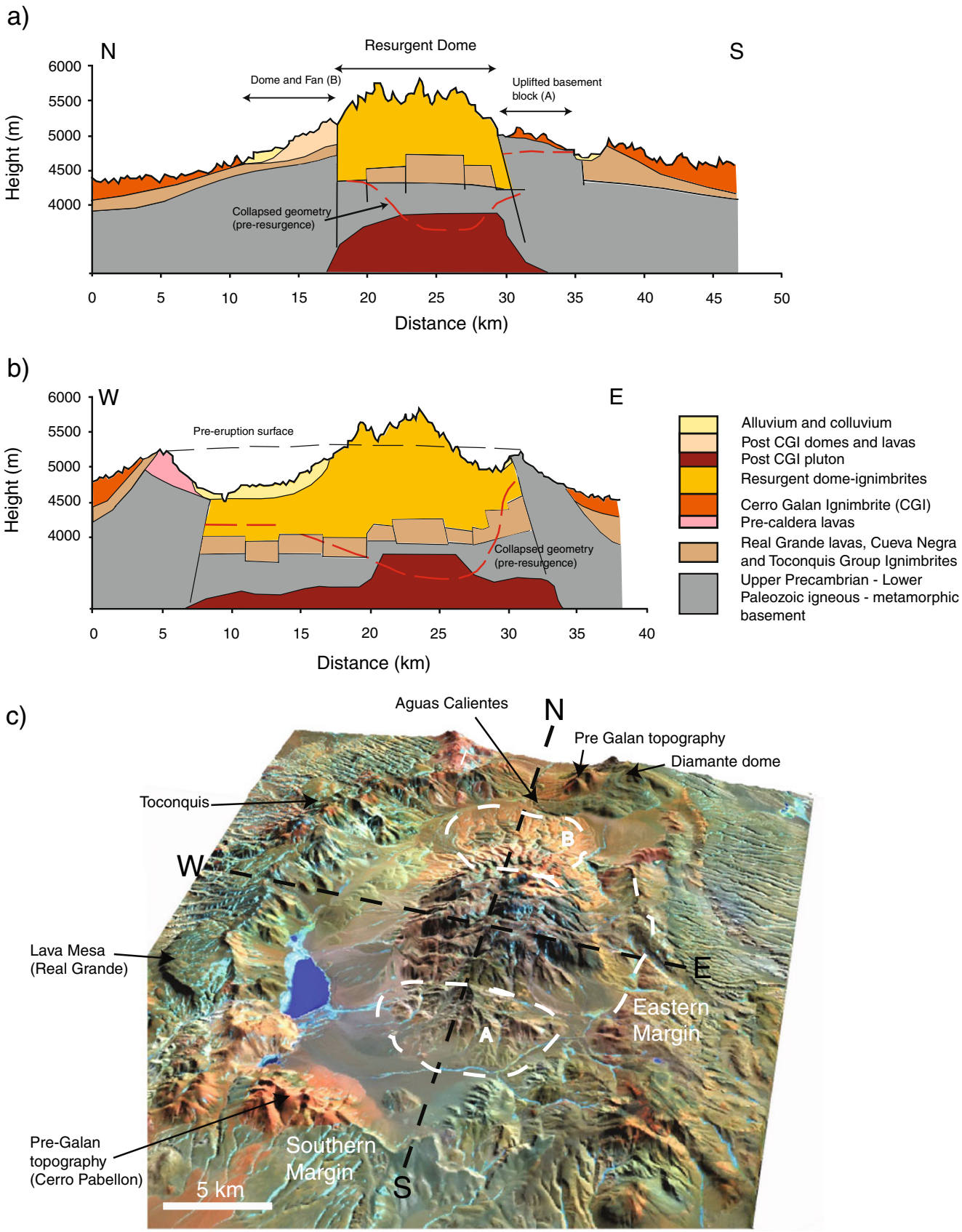
a)
N
S
Resurgent Dome
Dome and Fan (B)
Uplifted basement block (A)
Collapsed geometry (pre-resurgence)
Height (m)
6000
5500
5000
4500
4000
0
5
10
15
20
25
30
35
40
45
50
Distance (km)
b)
W
E
Pre-eruption surface
Collapsed geometry (pre-resurgence)
Height (m)
6000
5500
5000
4500
4000
0
5
10
15
20
25
30
35
40
Distance (km)
Alluvium and colluvium
Post CGI domes and lavas
Post CGI pluton
Resurgent dome-ignimbrites
Cerro Galan Ignimbrite (CGI)
Pre-caldera lavas
Real Grande lavas, Cueva Negra and Toconquis Group Ignimbrites
Upper Precambrian - Lower Paleozoic igneous - metamorphic basement
c)
Aguas Calientes
N
Pre Galan topography
Diamante dome
Toconquis
W
B
E
Lava Mesa (Real Grande)
A
Eastern Margin
Pre-Galan topography (Cerro Pabellon)
Southern Margin
S
5 km

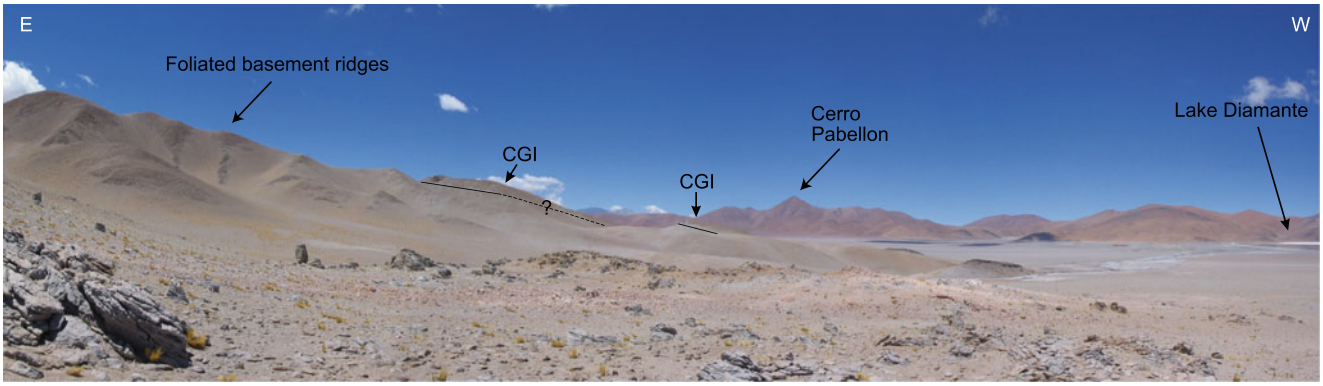

Fig. 10 Field photo showing the southern portion of the resurgent dome and southern caldera margins. Photo taken facing south

northern flank of the resurgent dome. We agree with this interpretation, but suggest that this resurgent-dome-bounding fault is the northern structural margin of the caldera (Fig. 11).

Caldera collapse mechanism

Our new observations suggest that the central elliptical depression bounded by N-S trending basement faults is not the topographic remnant of a caldera formed by 'the catastrophic foundering of a coherent cauldron block into the magma chamber' (Sparks et al. 1985). Instead, we suggest collapse was either piecemeal or fault-bounded trap-door style, hinged east of the current resurgent dome (Figs. 9 and 11).

We propose a model in which collapse was initially accommodated along N-S faults that define the western topographic margin of the caldera, at ~5,200 m, where the hinge line is currently marked by the eastern drainage divide also located at 5,200 m. The similarity in elevation to the west and east of the caldera depression indicate relatively flat pre-collapse topography, although regional tumescence associated with CGI magma emplacement may have produced a slight pre-eruptive doming. After initiation of caldera collapse, piecemeal breakup of the caldera floor may have produced the deeper collapse that propagated eastward to allow a minimum intracaldera CGI thickness of 1.4 km to accumulate. Subsequently, the central portion of intracaldera fill was uplifted to form a central resurgent dome. The difference in elevation between the eastern and western caldera floors is approximately 500–800 m, which lends further support to an asymmetric collapse mechanism. We conclude that all of the topography was created by differential collapse rather than differential uplift because of the elevation and dip coherence between the basement blocks on eastern and western margins. Resurgent block uplift appears to have been accommodated largely along the N-S and E-W faults, with structural doming extending into the basement forming the southern part of the resurgent block (Fig. 11).

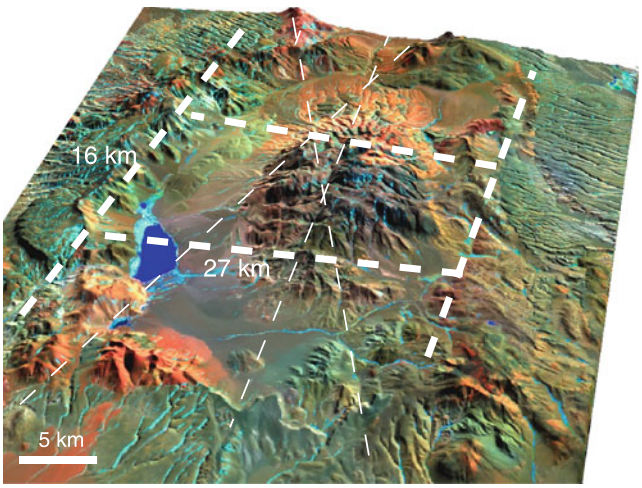

Fig. 11 ASTER 30 m DEM overlain with traces of major faults within the Galán depression. Bounding collapse faults shown as thick dashed lines. These define the rectangular region that is the collapse caldera. Other faults (from image interpretation) shown in lighter dashed lines (see also Chernicoff et al. 2002). See Fig. 9 for features and text for further details

The stratigraphy in the southern and northern margins of the resurgent dome is integral to the interpretation of piecemeal collapse. The presence of basement in the southernmost part of the resurgent dome, with just the thin veneer of CGI, implies that the southern part of the current Galán depression did not collapse. Therefore, slip must have been accommodated along the E-W fault that separates the southern basement-dominated portion from the main mass of the resurgent dome. Similarly, the northern collapse margin lies in an area now buried under the post-CGI dome complex, considerably inboard of the northern topographic margin. We suggest that an ESE-WNW regional fault akin to that identified by Chernicoff et al. (2002; a major regional lineament connecting the Toconquis massif across the northern part of the resurgent dome through the eastern hinge) bounded the collapsing block to the north. Further interpretation of the aeromag-

netic data for the central caldera region by Chernicoff et al. (2002) shows three overlapping anomalies that coincide with these areas: post-CGI domes and an associated volcaniclastic sequence to the north; the resurgent block; and the southern part of the Cerro Galán depression. The resulting fault-bounded collapse block thereby had an isosceles trapezoid outline and an area of ~450 km^2 (27× 16 km maximum dimensions). Assuming at least 1.4 km thickness of CGI in the resurgent block (Sparks et al. 1985), we suggest that a minimum average thickness of 1 km accumulated as intracaldera CGI. Using a reasonable volume ratio of 0.70 (for piecemeal-trapdoor collapse vs. purely plate- or piston-style collapse), we calculate that at least 315 km^3 of intracaldera CGI collected due to caldera collapse. Given the high density of intracaldera ignimbrite (high degrees of welding with <5% porosity), this would translate to approximately the same DRE volume.

We agree with Sparks et al. (1985) that the collapse of the Cerro Galán caldera was controlled by regional faults. However, we propose a new interpretation that the nature (and therefore shape) of the collapse was essentially of a piecemeal keystone graben form. The elliptical form of Cerro Galán is, then, an artifact of pre-existing topography and a stress field superimposed on the regional structural grain (caldera bounding N-S regional faults) by the Galán magmatic system. Late extrusions that utilized pre-existing fractures, modified by this stress field, may also contribute to the apparent ring fracture geometry, as is often assumed for calderas (Lipman 1997). These modifications notwithstanding, we concur with a model of outward-dipping faults accommodating the collapse and the eruption of the CGI (Fig. 9). This model, where large clean vents open rapidly as caldera collapse progresses, is consistent with the eruption of lithic-poor, dense pyroclastic flows that were continuously fed from dense columns that collapsed on inception (e.g., Sparks et al. 1985). Combining the central resurgent dome with the other centers that make up the Galán system (post-CGI domes and associated volcaniclastic deposits to the north of the dome, and the southern part of the Cerro Galán depression) and the clear role that regional faults have played, we propose that the entire Cerro Galán system area be defined as the Cerro Galán volcano-tectonic depression, the central part of which contains the Cerro Galán caldera *sensu strictu*.

Discussion

Revised volume estimations for the Galán ignimbrites

Accurate estimation of erupted volumes of large silicic pyroclastic sequences is difficult due to inherent assumptions about the loss of material due to lack of preservation and/or erosion. The 1,000 km^3 (DRE) erupted CGI volume estimate of Sparks et al. (1985), which included 280 km^3 outflow, 450 km^3 intracaldera ignimbrite and 330 km^3 co-ignimbrite ash, assumed an average outflow thickness of 62 m and an original areal extent of 7,500 km^2. The intracaldera ignimbrite volume was calculated using a caldera area of 450 km^2 and an intracaldera thickness of 1,000 m, the average height of the resurgent dome.

We revise these estimates based on new deposit maps and field observations. We extrapolate from preserved outflow deposit thickness and areal distribution, using three correction factors. Factor A accounts for lack of exposure or inaccessibility of field locations, which may cause an underestimation of preserved deposits. Factor B accounts for syn-eruptive loss of co-ignimbrite ash from the pyroclastic columns and pyroclastic flows. Factor C accounts for a decrease in deposit volume due to post-eruptive erosion. The corrected outflow sheet volume is then added to an estimated intracaldera deposit fill volume.

Few studies include correction factors A-C, the values of which are often approximated based on Lipman's (1984) assertion that the intracaldera fill, outflow sheet and co-ignimbrite ash have approximately equal volumes. This assumption has been applied for the Toba tuff (Rose and Chesner 1987) and the Oruanui ignimbrite (Wilson 2001), for example. Due to a lack of appropriate alternatives, the same correction factors and thereby an assumption of similar eruption, transport and erosion processes, have been assumed elsewhere (Mason et al. 2004). However, new work by Salisbury et al. (2010) on multiple ignimbrite deposits in the APVC has shown the volumes of intracaldera ignimbrites to exceed those found in their associated outflow sheets. Lindsay et al. (2001) speculated this was the case with the La Pacana caldera, where collapse occurred early in the eruption of the Atana Ignimbrite and up to two-thirds of the ignimbrite ponded in the caldera. Thus it appears that timing of collapse may be critical in the relative proportions of ignimbrite intracaldera fill and outflow sheet volumes.

Based upon our field observations and previous work by Sparks et al. (1985), deposit maps and average deposit thickness estimates were constructed for the currently preserved extent of the outflow sheet for each ignimbrite (Fig. 2b-d). Preserved areas range from 50 km^2 for the Cueva Negra Ignimbrite to 2,400 km^2 for the Cerro Galán Ignimbrite (Table 3). For the oldest Toconquis Group Ignimbrites (Blanco and the Merihuaca Formation), which were only logged at Rio de Las Pitas, the area was estimated using the thickness in this locality. For the more widely dispersed ignimbrites (Pitas, Real Grande, Cueva Negra and CGI), an average thickness was estimated from multiple localities.

Factor A compensates for the degree of deposit exposure, and the inaccessibility of potential depositional localities. A value of 1 for factor A indicates that all preserved material is exposed and has been observed. Based on the thickness of CGI deposits where the base of this ignimbrite is visible, we estimate that only two thirds of the CGI is currently exposed. We therefore attribute a factor A of 1.5±0.5 to the CGI (i.e., some of the deposit is certainly buried, but the buried volume is not more than 50% of the exposed volume; Table 3). The base of the CGI is rarely exposed in observed sections; therefore older ignimbrites are inferred to be buried beneath outcrops of CGI. We assume that the Cueva Negra Ignimbrite extends continuously from existing exposures to the north-east of the caldera (near the uranium mine) southward to the southernmost exposure at Rio Leon Muerto (Fig. 2c). We calculate that only ~25% of this ignimbrite is currently exposed and therefore give the Cueva Negra Ignimbrite a factor A of 4±1 (accounting for uncertainties in the distribution of buried ignimbrite). Using similar reasoning for the west and north of the caldera, and by using the CGI distribution as a proxy for likely valley-fill deposits, the Pitas and Real Grande Ignimbrites are given A=2.75±1 and the Merihuaca Formation and Blanco Ignimbrites A=1.75±0.5 (Table 3).

Co-ignimbrite plumes can be generated over the entire length of a pyroclastic flow and extend well beyond the extent of the resultant ignimbrite (Sparks et al. 1997). When this material is deposited, it may be quickly eroded and re-sedimented elsewhere, so that it is absent from the stratigraphy observed today. The best documented example of a co-ignimbrite plume from a large silicic ignimbrite eruption is that associated with the youngest Toba Tuff, which erupted ~75,000 years ago on the island of Sumatra. Detailed studies of deep sea tephra layers in the Bay of Bengal and ash layers on the Indian continent led to an estimated volume of co-ignimbrite ash-fall deposits of 800-1,000 km^3 (Ninkovich et al. 1978; Rose and Chesner 1987). This is approximately 29-36% of the total 2,800 km^3 (DRE) erupted volume. Similar studies of the 1991 eruption of Unzen (Watanabe et al. 1999) and the 1815 eruption of Tambora (Sigurdsson and Carey 1989) yield co-ignimbrite ash estimates that comprise 30–40% of the total erupted volume. Some authors have suggested that, for the largest ignimbrite eruptions, up to 50% of the total erupted volume may have been contained within these co-ignimbrite plumes (Woods and Wohletz 1991; Sparks et al. 1997).

The amount of co-ignimbrite ash originally generated from each pyroclastic flow in the Cerro Galan system (Factor B in Table 3) is difficult to estimate accurately. A factor B of 1 indicates that there has been no volume loss to co-ignimbrite ash deposits. The CGI, Cueva Negra and older Toconquis Ignimbrites exhibit little or no evidence for significant volumes of ash-fall preceding the emplacement of the large-volume ignimbrites. This suggests that the eruptions that produced these ignimbrites lacked a highly expanded, low density plinian-type eruption column. Thus most of the fine ash-sized material would have been carried within the pyroclastic flows as they traveled away from their source. Some elutriation of fine-ash likely took place during transport and subsequent flow emplacement; this would have created co-ignimbrite plumes that carried the finest particles far beyond the maximum extent of the ignimbrites (e.g., Sparks and Walker 1977).

Because the dominant proportion of crystals in the matrix is larger than fine ash size, fine ash elutriation may result in a relative reduction in the proportion of glassy ash in the ignimbrite matrix relative to the proportion of glass in pumice clasts. Crystal enrichment from fine ash and/or glass loss in ignimbrite matrix relative to pumice clasts was first documented by Lipman (1967) on Aso caldera, Japan, where the deposited ignimbrites appeared to represent only half of the erupted volume. This phenomenon has since been identified in many other ignimbrites, and typically yields an upper value of 50% depletion of fine ash from the ignimbrite matrix (Walker 1972). We have applied this method by point counting thin sections of co-existing matrix and juvenile clasts in the CGI (Table 1 in electronic supplementary material). At distal localities of the eastern and western ignimbrite outflow sheet, matrix ash is depleted by 17–34%. However, the variability in pumice crystallinity (Folkes et al. 2011) indicates that these values are preliminary approximations only.

We have not observed any distal ash-fall deposits beyond the currently-preserved ignimbrite deposits associated with the Galán caldera. The Toba Dacitica (2.78±0.09 Ma) of Marshall and Patterson (1981), which was suggested as a possible co-ignimbrite ash deposit of the CGI (Sparks et al. 1985), contains hornblende and pyroxene, inconsistent with the CGI mineralogy (S. Hildyard pers. comm.). Because correlative distal ash-fall deposits from the Cerro Galán region have not been identified, based on our crystal enrichment data, we estimate a value of 33±10% (Factor B=1.5±0.25; Table 3) ash loss from all of the Galán ignimbrites. The uncertainty in this factor reflects variations in pumice proportion and sizes between different Galán Ignimbrites. This range overlaps with the estimates for the systems described above.

The accuracy in estimates of erosive loss (Factor C) is highly variable among ignimbrite deposits because of variation in deposit age and estimates of erosion rates. A factor C of 1 indicates that there has been no post-depositional erosion. We assume that erosion affected all of the ignimbrites. For example, at the most distal extent of the preserved CGI on both the eastern and western margins,

the ignimbrite is at least 40 m thick. We assume that the original deposit thickness at its maximum runout distance was less than this value, implying significant headward erosion of the distal deposit margins.

The erosion rates in the Central Andean Puna region are difficult to estimate because wind is the primary cause of erosion, with minor fluvial erosion confined to sparse drainage basins. Strecker et al. (2007) showed that the Central Andes of northern Chile have been arid or semi-arid since ~6.4 Ma, therefore we assume that erosion rates depend primarily on repose periods between ignimbrite eruptions. The amount of erosion also depends on the type of eroding material, with very different erosion rates for ignimbrites than lavas, for example. Original structures in basaltic andesite volcanoes in the Galán region dated at 1.6–2.5 Ma (e.g., Los Nacimientos, El Jote, North Hombre Muerto; Risse et al. 2008) are well preserved, suggesting very limited erosion.

The amount of post-depositional erosion can be estimated for the CGI by comparing deposit thicknesses within a single valley. To the north of the caldera, just south of the Salar del Hombre Muerto, a series of parallel 'yardangs' or elongate ridges have been created by wind erosion. Here, as much as two thirds of the CGI appears to be missing through erosion. In contrast, other localities around the caldera show little evidence of CGI erosion. To calculate volume loss, we have compared the elevations of preserved ignimbrite deposits along valley margins with those in the valley axes using satellite images and elevation data, and approximate that one half (50%) of the CGI is missing. This yields a factor C for the CGI of 2±0.25 (Table 3). It is difficult to apply the same observations to the older Galán Ignimbrites because of their burial below the CGI in many localities. We therefore estimate the degree of erosion for these ignimbrites based on the repose periods between eruptions. For deposits with post-eruptive repose intervals of greater than 0.5 Myr (the CGI, Cueva Negra and Real Grande Ignimbrites), we attribute a factor C of 2±0.25. For deposits with post-eruptive repose intervals of less than 0.5 Myr (the Pitas, Merihuaca Formation and Blanco Ignimbrites), we attribute a factor C of 1.5±0.25 (Table 3). The uncertainties in factor C for these older ignimbrites also reflect the variations in their textures (i.e., degree of welding or induration).

Based on factors A, B and C, we have calculated new (bulk) volume estimates (with maximum and minimum values based on uncertainties) for all the ignimbrite outflow sheets (Table 3). Given the bulk outflow volumes of the older Galán Ignimbrites (~10 to 500 km^3) and the shallow nature of their associated magma chambers (<10 km; see Folkes et al. 2011), some degree of crustal collapse would likely have occurred during each eruption, resulting in intracaldera equivalents associated with each documented outflow sheet. However, the eruption and deposition of the CGI in the present-day caldera has largely obscured intracaldera fill portions of the older Galán Ignimbrites. We assume that intracaldera fill forms the same proportion (about 50% of the total volume; consistent with Lindsay et al. 2001 and Salisbury et al. 2010 for other large collapse calderas in the Central Andes) of total erupted volume for the older ignimbrites, with the caveat that this value may have been slightly different for each eruption due to the form and timing of caldera collapse.

Finally, total erupted volumes (the sum of intracaldera and outflow volumes) are normalized to dense rock equivalent (DRE) volumes. DRE volumes are based on a magma density (water-free) of 2,450 kg/m^3 (Folkes et al. 2011), and an average solid rock density of 2,400 kg/m^3 for the welded intracaldera CGI, 1,600 kg/m^3 for the CGI outflow sheet, 2,000 kg/m^3 for the welded Cueva Negra Ignimbrite and 1,500 kg/m^3 for the less indurated Toconquis Group Ignimbrites. Therefore, from a total bulk volume of ~800 km^3 (315 km^3 intracaldera and 486 km^3 corrected outflow volume), the DRE volume of the CGI is found to be ~630 km^3 (Table 3; error range is 460 to 860 km^3), approximately two thirds of that proposed by Sparks et al. (1985).

Sparks et al. (1985) estimated that the entire Toconquis Group Ignimbrites totaled 400–500 km^3 (DRE), with the Real Grande Ignimbrite comprising one-half to two thirds of this volume (Fig. 12a). Based on our updated estimates, the total volume of the Toconquis Group is ~650 km^3 (DRE) with the Real Grande Ignimbrite comprising ~390 km^3 (error range 300 to 560 km^3), ~60% of this total (Table 3). Moreover, our data show that the Galán system has erupted progressively larger volumes of material over this ~3 Myr time period (Fig. 12b). The oldest eruptions (the Blanco and Merihuaca Formation) produced four medium-sized ignimbrites (total volume of ~70 km^3 DRE) over <0.2 Myr. This is in contrast to the younger Pitas, Real Grande, Cueva Negra and CGI Ignimbrites, which erupted a combined volume of 1,260 km^3 (DRE) with repose periods up to 1.2 Myr between each eruption. These longer periods of quiescence between eruptions may reflect the build-up of larger magma volumes in the upper crust, although this is not a linear relationship (Fig. 12b).

Lipman (2007) has shown that early stages of magma chamber growth in long-lived silicic systems may be characterized by successive eruptions of small to moderate volumes. To reach very large volumes, systems are often driven by elevated thermal fluxes combined with an episodic addition of sheet-like magma intrusions (Annen et al. 2008). Magma accumulation may proceed episodically, punctuated by a series of smaller-volume eruptions. The development of larger volume chambers then depends upon competing processes of chamber growth, energy

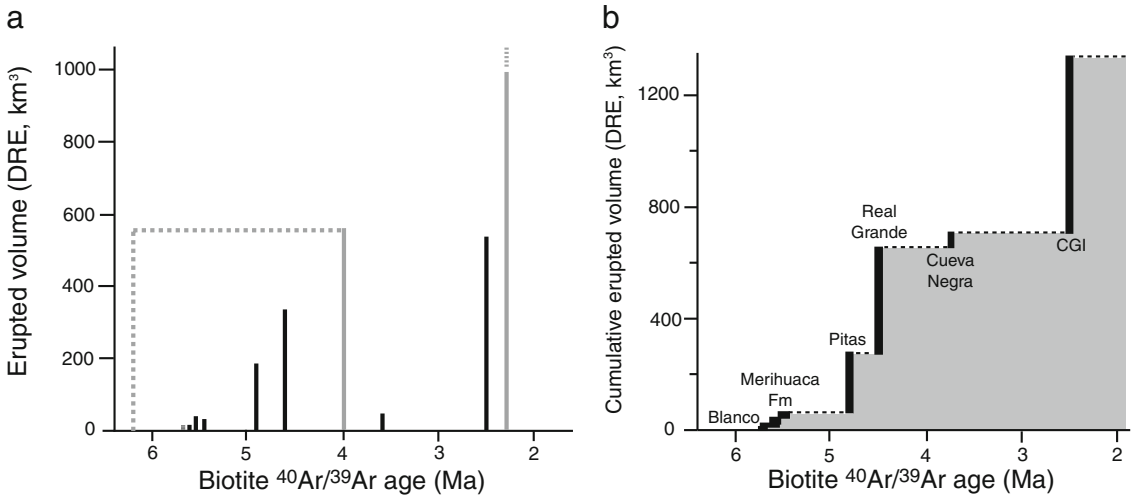

Fig. 12 **a**. New volume estimates for the Galán Ignimbrites (black bars). Previous volume estimates by Sparks et al. (1985) are shown as grey bars. Note: the previous estimates grouped the entire Toconquis Group Ignimbrites into a single volume. **b** A cumulative volume-time graph of the Galán Ignimbrites

provided by magmatic volatiles (from the exsolution of H_2O, CO_2 and other gases at shallow depths), and thermal and mechanical constraints of the host rock material (e.g., Jellinek and DePaolo 2003). The increase in magma volumes over time at Cerro Galán could be explained by the changing physical properties of the upper crust into which these magmas were accumulating. In the nearby APVC of the Central Andes (~200 km north of Cerro Galán; Fig. 1), de Silva and Gosnold (2007) have shown that magmatism occurred in pulses between ~10–4 Ma, becoming more voluminous over time. These authors suggest that a combination of increased mantle input, increased magma production, and upward migration of the magmatic system, resulted in a combined 'thermomechanical' evolution of the upper crust in this area, promoting the accumulation of larger bodies of magma over time into host rock that was hotter and more ductile than during initial magmatic intrusions. Our observations at Cerro Galán are consistent with this model, whereby the more voluminous Real Grande and CGI magma bodies accumulated in thermally and mechanically 'primed' crust by the repeated accumulation and eruption of the older, smaller volume ignimbrite magmas.

The history of erupted volumes of ignimbrites at Cerro Galán and the APVC is marked by the rapid onset of voluminous ignimbrite eruptions, a sustained period (many millions of years) of large volume ignimbrite eruptions interspersed with periods of relative quiescence and a corresponding sharp cessation of voluminous eruptive activity. These events may be consistent with a 'pulse' in mantle activity, causing elevated magma fluxes in the lower crust (e.g., de Silva et al. 2006), and perhaps a consequence of lower crustal delamination in this region (e.g., Kay et al. 1994). Recent teleseismic topographic evidence by Heit (2005) records a thermal anomaly beneath Galán, which may be a result of such increased thermal and magma flux to the lower lithosphere.

The most recent post-caldera activity in the Cerro Galán region is the extrusion of small monogenetic basaltic-andesitic domes around the town of Antofagasta de La Sierra ~35 km west of the structural margin. These domes have been dated at 1.5 to 0.3 Ma (Risse et al. 2008), indicating ongoing activity of the Galán magmatic system. These ages, along with the ages of small-volume pre- and post-caldera lava flows, domes and pyroclastic deposits suggest the Cerro Galán magmatic system was active between the episodic eruptions of large volume ignimbrites. This implies that there has been a continual supply of magma to the upper crust at least from ~6 Ma to recent. We suggest the smaller volume 'inter-ignimbrite' deposits reflect the normal, 'steady-state' magma flux in the Cerro Galán system and that the eruption of large volume ignimbrites represent heightened fluxes of magmatic and thermal activity originating deeper in the crust and producing voluminous magmas that rise and accumulate in upper crustal magma chambers (cf. de Silva et al. 2006).

Implications for the physical volcanology of the Galán Ignimbrites

The Galán Ignimbrites share many similarities with other large-volume ignimbrites, but there are also differences. We address these similarities and differences by discussing the relative depositional characteristics, lithic-content, crystallinity, and pumice sizes and proportions of the Galán Ignimbrites in the context of each other and of silicic systems in general. Hildreth (1981), de Silva (1989a) and Ort (1993) report that crystal-rich, large-volume ignimbrites

commonly lack an initial Plinian fallout deposit, consist of a single, massive, widely-dispersed outflow ignimbrite and are typically indurated throughout most of their extent. These characteristics are common to many of the ignimbrites at Cerro Galán and led Sparks et al. (1985) to suggest that the CGI required very high eruption rates, achieved by foundering of the roof of the magma chamber into the magma body, causing eruption along ring faults. Ort (1993) and de Silva et al. (2006) suggest a similar eruption mechanism for many of the large APVC ignimbrites. We suggest that the absence of widespread fallout deposits in many of the Galán Ignimbrites requires either that the eruption columns never reached heights that were able to disperse the fine ash- and lapilli-sized material radially from the source, or/and that the onset of column collapse occurred almost immediately upon commencement of the eruptions. The low average vesicularity and minimum vesicularity of erupted clasts (Wright et al. 2011) is consistent with a dense eruption cloud of this type.

There is, however, evidence for thin ashfall layers at the base of the Real Grande and Lower Merihuaca Ignimbrites suggesting that a short-lived Plinian or sub-Plinian eruption column did exist upon the inception of eruption of these ignimbrites. We suggest that ignimbrites with a basal ashfall layer were able to sustain a Plinian or sub-Plinian eruption column early in their eruption, whereas the ignimbrites where this is absent (e.g., the CGI) originated from a sustained, low fountaining ('boil over') eruption. Sparks et al. (1985) speculated that the lack of a basal Plinian fallout in the CGI also required extremely high eruption rates facilitated by caldera collapse and rapidly widening outward dipping ring faults. Alternatively, fallout from larger eruptions may have been incorporated into widespread density currents and is not preserved (e.g., Branney and Kokelaar 2002). The ignimbrites with basal ashfall layers originated from more 'normal' eruption conditions creating eruption columns that were able to disperse fine ash- and lapilli-sized material westwards for at least 20 km. The CGI, Pitas and Upper Merihuaca Ignimbrites are proposed to have originated from a more complex eruption style, consisting of multiple source vents related spatially to the propagation of caldera collapse.

The presence of pumice concentration zones (PCZ's) in the Toconquis Group Ignimbrites and pumice-rich lenses in the CGI suggest pulsation in pyroclastic flows. These features likely represent the upper portions of individual pyroclastic flows, whereby the coarse, vesicular, low density pumice clasts rose buoyantly to the top of individual flow lobes as pumice 'flotsam' (e.g., Branney and Kokelaar 2002 and references therein). These PCZ's were then overridden by the next pulse of the pyroclastic flow producing a repeated deposit package capped by another PCZ. The lack of evidence for significant time breaks (e.g., absence of paleosol layers), between these PCZ's and the overlying ignimbrite deposits, suggests each subsequent flow event occurred over short timescales (hours to days). The pumice-rich lenses in the CGI are less laterally extensive, and thinner than the PCZ's in the Toconquis Group Ignimbrites and may represent the original distal extents of flow lobes, where pumice clasts are deposited as terminal pumice 'dams' or lateral pumice 'levees' (Branney and Kokelaar 2002). These pumice-rich deposits would have then been overridden by subsequent pyroclastic flows that were able to travel to more distal locations, creating the pumice lenses currently exposed in outcrop.

We also observe a very low abundance of lithic fragments (generally <2% by volume) within the CGI, the majority of which are likely accidental clasts interpreted to have been eroded and entrained from local basement and other pre-existing volcanic deposits. In contrast, older Galán Ignimbrites contain higher proportions of lithics. We agree with the interpretations of Sparks et al. (1985), who suggest that this decrease in lithic content was the result of extremely high eruption rates for the CGI (greater than for Toconquis Group Ignimbrites) along a large set of outward-dipping faults, for which conduit erosion was limited by caldera widening with progressive collapse-block foundering (the lack of a Plinian-like fallout deposit in the CGI supports the inference of a higher eruption rate). Furthermore, the greatest amount of caldera subsidence during the CGI eruption was focused along the western structural margins of the caldera, producing dramatic topography which may have prevented large or dense material from escaping the proximal caldera region.

The high abundance of crystals in the Galán Ignimbrites (juvenile clasts with >45% crystals on a vesicle-free basis) is explained by their storage and growth in shallow magma chambers. Evidence from mineral barometry shows that the Galán Ignimbrites contain a population of crystals that equilibrated and crystallized from magmas in the upper 10 km of the crust (<3 kbar; Folkes et al. 2011). This is consistent with recent work proposing that silicic ignimbrites with high crystal contents come from long-lived, non-zoned magma chambers (Bachmann and Bergantz 2004; Christiansen 2005). These highly viscous crystal 'mushes' are sometimes erupted as non-zoned crystal-rich ignimbrites, but more commonly remain as granodioritic batholiths. Large accumulations of 'homogenized' magma are created by a combination of processes including recharge of magma with similar compositions to the accumulating magma, efficient blending or stirring of this recharge magma, and the suppression of crystal-melt segregation (Bachmann and Bergantz 2008). Long-lived crystal mush zones are thought to be sustained by continual injections of magma into the middle and upper crust, sustaining magma

residence times of $>10^5$ years (Bachmann and Bergantz 2004). We agree with this model for the Galán Ignimbrites and suggest that a crystal-rich mush zone existed throughout the eruption period of the Galán Ignimbrites, and that is was repeatedly recharged with compositionally-identical magma from deeper levels in the crust (Folkes et al. 2011).

An important feature of the CGI is its relatively low pumice content (generally <10% by volume) and smaller average pumice size (clasts generally <10 cm in diameter) compared with the older Toconquis Group Ignimbrites (20–40% by volume, average clast diameter of ~20 cm). This is a characteristic textural difference between the ignimbrites, and its origin therefore requires special attention. We suggest that a combination of factors promoted greater amounts of fragmentation (and therefore smaller pumice clasts) in the CGI eruption compared to that during the eruptions of the older Toconquis Group Ignimbrites. Firstly, magmatic temperatures of the CGI (<790°C) are slightly lower than those for the older ignimbrites (>790°C; Folkes et al. 2011), indicating that the CGI magma would have been closer to the glass transition temperature. It was therefore able to behave in a more brittle manner, resulting in a greater degree of fragmentation. Secondly, the extremely high eruption rates that were required to produce the CGI and coincident high decompression rates may have contributed to greater fragmentation of juvenile clasts during eruption. Finally, these high eruption rates would have produced higher exit velocities and turbulence in the pyroclastic density currents that produced the CGI, resulting in greater amounts of clast to clast contact and mechanical fragmentation within the CGI pyroclastic density currents than for the older ignimbrites.

Conclusions

Our new biotite $^{40}Ar/^{39}Ar$ age determinations coupled with paleomagnetic data and field and stratigraphic observations have resulted in some important revisions of the volcanism and stratigraphy associated with the Cerro Galán system. The main results are as follows:

1. The Cerro Galán system has erupted nine major ignimbrites since ~6 Ma. Biotite $^{40}Ar/^{39}Ar$ ages show that two ignimbrites; the Pitas (4.84±0.04 Ma) and Vega (4.51±0.11 Ma) Ignimbrites can now be distinguished. The Cueva Negra Ignimbrite (3.77±0.08 Ma) is distinct from the Real Grande Ignimbrite (4.68±0.06 Ma).
2. The extent of some of the older Toconquis Group Ignimbrites is greater than previously documented. The Real Grande and Pitas Ignimbrites are found to the southwest (Rio Pirica) and north (Ojo de Ratones) of the caldera. The currently-preserved areal extent of the Toconquis Group Ignimbrites ranges from ~220–420 km^2.
3. New mapping and interpretation of satellite images allows a re-interpretation of the caldera margins and form of collapse. The caldera is strongly fault controlled. The northern and southern margins of the caldera are now identified as fault bounded margins on the edge of the resurgent block. Collapse was accommodated in a piecemeal trapdoor fashion along a regional N-S fault that defines the western margin of the caldera with a hinge along a N-S regional fault in the east. The collapse was locally as deep as at least 1.4 km beneath the area now occupied by the resurgent block, equal to the thickness of CGI within the resurgent center.
4. The extent of the CGI quoted by Francis et al. (1983) and Sparks et al. (1985) is an overestimate. This ignimbrite is found 40 km in all directions from the structural margins, with a maximum distal extent of ~80 km. Based on detailed mapping and field observations, we report that the currently-preserved areal extent of the CGI is ~2,400 km^2.
5. Revised volume estimates show that the 1,000 km^3 (DRE) of magma inferred to have produced the CGI (Sparks et al. 1985) is an overestimate. Based on more thorough analyses of volume estimation factors, we find that the CGI had a magmatic volume of ~630 km^3 (DRE), of which approximately half is intracaldera fill.
6. Magma volumes increased with subsequent eruptions in the Galán volcanic system, perhaps reflecting the thermo-mechanical evolution of the upper crust in response to the older Toconquis Group ignimbrite magmas 'priming' the crust for accumulation of larger batholith-sized chambers (the Real Grande and CGI magmas).
7. The Cerro Galán system has experienced significant volcanic activity in the time periods between the eruptions of the nine large-volume ignimbrites. Evidence for numerous lava flows, silicic dome extrusions, pyroclastic flows and surges, and young basaltic-andesite scoria cones suggests that magmatic and volcanic activity has been continuous since ~6 Ma. The large-volume ignimbrites represent increased thermal and magmatic fluxes to the upper crust in the period before the eruption of these crystal-rich silicic deposits.

Acknowledgements This research was funded by an Australian Research Council Discovery Program Grant DP0663560 to the research team led by R. Cas. We thank Monash University, Oregon State University, Universita di Roma Tre and Salta University for access to the various facilities required to undertake this research. J.G. Viramonte wishes to thank Agencia de Promoción Científica y Tecnologica, MINCyT, Argentina, Grant PICT BID-1728 OC/AR 38131. Journal reviews from Steve Sparks, Michael Ort and William McIntosh and suggestions from the editors for this special issue helped to improve this manuscript.

References

Annen C, Pichavant M, Bachmann O, Burgisser A (2008) Conditions for the growth of a long-lived shallow crustal magma chamber below Mount Pelee volcano (Martinique, Lesser Antilles Arc). J Geophys Res 113(B07209, doi:10.1029/2007JB005049)

Bachmann O, Bergantz GW (2004) On the origin of crystal-poor rhyolites: Extracted from batholithic crystal mushes. J Petrol 45:1565–1582

Bachmann O, Bergantz GW (2008) Deciphering Magma Chamber Dynamics from Styles of Compositional Zoning in Large Silicic Ash Flow Sheets. Rev Mineral Geochem 69:651–674

Branney MJ, Kokelaar P (2002) Pyroclastic Density Currents and the Sedimentation of Ignimbrites. Geol Soc London Mem 27: pp 152

Cande SC, Kent DV (1995) Revised calibration of the geomagnetic polarity timescale for the Late Cretaceous and Cenozoic. J Geophys Res 100(B4):6093-6095

Chernicoff CJ, Richards JP, Zappettini EO (2002) Crustal lineament control on magmatism and mineralization in northwestern Argentina: geological, geophysical, and remote sensing evidence. Ore Geol Rev 21:127–155

Christiansen EH (2005) Contrasting processes in silicic magma chambers: evidence from very large volume ignimbrites. Geol Mag 142(6):669–681

Coira B, Caffe P, Kay SM, Diaz A, Ramirez CF (1996) Complejo volcanico Vilama-Sistema calderico del Cenozoico superior en Puna. Jujuy. XIII Congreso Geologico Argentino, Actas III, pp 603–620

Coira BL, Davidson J, Mpodozis C, Ramos VA (1982) Tectonic and magmatic evolution of the Andes of northern Argentina and Chile. Earth Sci Rev 18:303–332

de Silva S (1989a) Altiplano-Puna volcanic complex of the central Andes. Geology 17:1102–1106

de Silva S (1989b) Geochronology and stratigraphy of the ignimbrites from the 21°30'S to 23°30′S portion of the Central Andes of northern Chile. J Volcanol Geotherm Res 37:93–131

de Silva SL, Francis PW (1989) Correlation of large ignimbrites; two case studies from the Central Andes of northern Chile. J Volcanol Geotherm Res 37(2):133–149

de Silva SL, Francis PW (1991) Volcanoes of the Central Andes. Springer, Heidelberg, p 263

de Silva SL, Gosnold WD (2007) Episodic construction of batholiths: Insights from the spatiotemporal development of an ignimbrite flare-up. J Volcanol Geotherm Res 167:320–335

de Silva SL, Zandt G, Trumbull R, Viramonte JG, Salas G, Jimenez N (2006) Large ignimbrite eruptions and volcano-tectonic depressions in the Central Andes: a thermomechanical perspective. In: Troise C, de Natale G, Kilburn CRJ (eds) Mechanisms of activity and unrest at large caldera. Geological Society, London, Special Publications, pp 47–63

Folkes CB, de Silva SL, Wright HM, Cas RAF (2011) Geochemical homogeneity of a long-lived, large silicic system; evidence from the Cerro Galan caldera, NW Argentina. Bull Volcanol

Francis PW, Baker MCW (1978) Sources of two large volume ignimbrites in the Central Andes: Some Landsat evidence. J Volcanol Geotherm Res 4:81–87

Francis PW, O'Callaghan LJ, Kretschmar GA, Thorpe RS, Sparks RSJ, Page RN, de Barrio RE, Gillou G, Gonzalez OE (1983) The Cerro Galan ignimbrite. Nature 301:51–53

Friedman JD, Heiken G (1977) Report in: Skylab explores the Earth. NASA Pub 380:137–170

Gardeweg M, Ramirez CF (1987) The La Pacana caldera and Atana ignimbrite—a major ash-flow and resurgent caldera complex in the Andes of Northern Chile. Bull Volcanol 49:547–566

Gonzalez OE (1984) Las ignimbritas de "Ojo de Ratones" y sus relaciones regionales, provincia de Salta. Nov Cong Geol Arg Actas I:206–220

Guest JE (1969) Upper Tertiary Ignimbrites in the Andean Cordillera of Part of the Antofagasta Province, Northern Chile. Geol Soc Am Bull 80(3):337–362

Heit B (2005) Teleseismic tomographic images of the Central Andes at 21° S and 25.5° S: an inside look at the Altiplano and Puna Plateaus (PhD thesis). In: Freie Universitat. Berlin, p 137

Hildreth W (1981) Gradients in silicic magma chambers: implications for lithospheric magmatism. J Geophys Res 86:10153–10192

Hora JM, Singer BS, Jicha BR, Beard BL, Johnson CM, de Silva S, Salisbury M (2011) Volcanic biotite-sanidine $^{40}Ar/^{39}Ar$ age discordances reflect Ar partitioning and pre-eruption closure in biotite. Geology 38(10):923–926

Jellinek AM, DePaolo DJ (2003) A model for the origin of large silicic magma chambers: precursors of caldera-forming eruptions. Bull Volcanol 65:363–381

Jordan TE, Isacks BL, Allmendinger RW, Brewer JA, Ramos VA, Ando CJ (1983) Andean tectonics related to geometry of the subducted Nazca plate. Geol Soc Am Bull 94:341–361

Kay SM, Coira B, Viramonte J (1994) Young mafic back arc volcanic rocks as indicators of continental lithospheric delamination beneath the Argentine Puna plateau, central Andes. J Geophys Res 99(B12):24323–24339

Kay SM, Mpodzis C, Coira B (1999) Neogene magmatism, tectonism, and mineral deposits of the Central Andes (22° to 33°S latitude). In: Skinner BJ (ed) Geology and Ore deposits of the Central Andes, Society of Economic Geologists Special Publication. pp 27–59

Kay SM, Coira B, Worner G, Kay RW, Singer BS (2011) Geochemical, isotopic, and single crystal $^{40}Ar/^{39}Ar$ age constraints on the evolution of the Cerro Galan Ignimbrites. Bull Volcanol, doi:10.1007/s00445-010-0410-7

Koppers AAP (2002) Software for $^{40}Ar/^{39}Ar$ age calculations. Comput Geosci 28:605–619

Lesti C, Porreca M, Giordano G, Mattei M, Cas RAF, Wright HM, Viramonte J (2011) High temperature emplacement of the Cerro Galán and Toconquis Group Ignimbrites (Puna plateau, NW Argentina) determined by TRM analyses. Bull Volcanol

Lindsay JM, de Silva S, Trumbull R, Emmermann R, Wemmer K (2001) La Pacana caldera. N Chile: a re-evaluation of the stratigraphy and volcanology of one of the world's largest resurgent calderas J Volcanol Geotherm Res 106:145–173

Lipman PW (1967) Mineral and Chemical Variations within an Ash-flow Sheet from Aso Caldera, Southwestern Japan. Cont Min Petrol 16:300–327

Lipman PW (1984) The roots of ash flow calderas in western north America: windows into the tops of granitic batholiths. J Geophys Res 89((B10)):8801–8841

Lipman PW (1997) Subsidence of ash-flow caldera: relation to caldera size and magma-chamber geometry. Bull Volcanol 59:198–218

Lipman PW (2007) Incremental assembly and prolonged consolidation of Cordilleran magma chambers: Evidence from the Southern Rocky Mountain volcanic field. Geosphere 3(1):42–70

Marshall LG, Patterson B (1981) Geology and geochronology of the mammal-bearing Tertiary of the Valle de Santa Maria and Rio Corral Quemado, Catamarca Province, Argentina. Fieldiana, Geol 1321:1–80

Mason BG, Pyle DM, Oppenheimer C (2004) The size and frequency of the largest explosive eruptions on Earth. Bull Volcanol 66:735–748

Ninkovich D, Sparks RSJ, Ledbetter MJ (1978) The exceptional magnitude and intensity of the Toba eruption, Sumatra: an example of the use of deep sea tephra layers as a geological tool. Bull Volcanol 41:286–298

Ort MH (1993) Eruptive processes and caldera formation in a nested downsag-collapse caldera, Cerro Panizos, central Andes mountains. J Volcanol Geotherm Res 56(3):221–252

Quane SL, Russell JK (2005) Ranking welding intensity in pyroclastic deposits. Bull Volcanol 67:129–143

Renne PR, Swisher CC, Deino AL, Karner DB, Owens TL, DePaolo DJ (1998) Intercalibration of standards, absolute ages and uncertainties in $^{40}Ar/^{39}Ar$ dating. Chem Geol 145:117–152

Riller U, Petrinovic I, Ramelow J, Strecker M, Oncken O (2001) Late Cenozoic tectonism, collapse caldera and plateau formation in the central Andes. Earth Planet Sci Lett 188:299–311

Risse A, Trumbull RB, Coira B, Kay SM, van den Bogaard P (2008) $^{40}Ar/^{39}Ar$ geochronology of the mafic volcanism in the back-arc region of the southern Puna plateau, Argentina. J S Am Earth Sci 26:1–15

Rose WI, Chesner CA (1987) Dispersal of ash in the great Toba eruption, 75 ka. Geology 15:913–917

Salfity JA (1985) Lineamentos transversales al rumbo andino en el Noroeste Argentino. Actas del 4. Congreso Geologico Chileno 2: A119–A127

Salisbury MJ, Jicha BR, de Silva SL, Singer BS, Jimenez NC, Ort MH (2010) $^{40}Ar/^{39}Ar$ chronostratigraphy of Altiplano-Puna volcanic complex ignimbrites reveals the development of a major magmatic province. Geol Soc Am Bull doi:10.1130/B30280.1

Sigurdsson H, Carey S (1989) Plinian and co-ignimbrite tephra fall from the 1815 eruption of Tambora volcano. Bull Volcanol 51:243–270

Smith RL, Bailey RA (1966) The Bandelier Tuff—a study of ash-flow eruption cycles from zoned magma chambers. Bull Volcanol 29:83–104

Soler M, Caffe P, Coira B, Onoe A, Kay S (2007) Geology of the Vilama caldera: a new interpretation of a large scale explosive event in the Central Andean plateau during the Upper Miocene. J Volcanol Geotherm Res 164(1–2):27–53

Sparks RSJ, Walker GPL (1977) The significance of crystal-enriched air-fall ashes associated with crystal-enriched ignimbrites. J Volcanol Geotherm Res 2:329–341

Sparks RSJ, Francis PW, Hamer RD, Pankhurst RJ, O'Callaghan LO, Thorpe RS, Page RN (1985) Ignimbrites of the Cerro Galan caldera, NW Argentina. J Volcanol Geotherm Res 24:205–248

Sparks RSJ, Bursik MI, Carey SN, Gilbert JS, Glaze LS, Sigurdsson H, Woods AW (1997) Volcanic Plumes. Wiley, p 574

Strecker MN, Alonso RN, Bookhagen B, Carrapa B, Hilley GE, Sobel ER, Trauth MH (2007) Tectonics and Climate of the Southern Central Andes. Ann Rev Earth Plan Sci 35:747–787

Taylor JR (1997) An Introduction to Error Analysis: The Study of Uncertainties in Physical Measurements. Mill Valley, California, p 327

Viramonte JG, Petrinovic IA (1990) Calderas asociades a megafracturas transcurrentes en los Andes Centrales del Sur. XI Congreso Geológico Argentino. San Juan. Actas II:369–372

Viramonte JG, Galliski MA, Saavedra V, Aparicio A, García Cacho L, Escorza M (1984) El finivulcanismo básico de la Depresión de Arizaro, provincia de Salta, República Argentina. IX Congreso Geológico Argentino, Actas III:234–254

Walker GPL (1972) Crystal Concentration in Ignimbrites. Cont Min Petrol 36:135–146

Watanabe K, Ono K, Sakaguchi K, Takada A, Hoshizumi H (1999) Co-ignimbrite ash-fall deposits of the 1991 eruptions of Fugendake, Unzen volcano, Japan. J Volcanol Geotherm Res 89:95–112

Wilson CJN (2001) The 26.5 ka Oruanui eruption, New Zealand: an introduction and overview. J Volcanol Geotherm Res 112:133–174

Woods AW, Wohletz K (1991) Dimensions and dynamics of co-ignimbrite eruption columns. Nature 350:225–227

Wright HMN, Folkes CB, Cas RAF, Cashman KV (2011) Heterogeneous pumice populations in the 2.56 Ma Cerro Galan ignimbrite: implications for magma recharge and ascent preceding a large volume silicic eruption. Bull Volcanol

York D (1969) Least squares fitting of a straight line with correlated errors. Earth Planet Sci Lett 5:320–324